

# Practical Convergence-Divergence Checks for Stresses from FEA

G.B. Sinclair

Department of Mechanical Engineering, Louisiana State University,  
Baton Rouge, LA 70803

J.R. Beisheim

Development Department, ANSYS Inc., Canonsburg, PA 15317

S. Sezer

Department of Mechanical Engineering, Louisiana State University,  
Baton Rouge, LA 70803

## Abstract

In practice in finite-element stress analysis, the engineer first needs to know if key stresses are converging, and second if they have converged to a reasonable level of accuracy. Then these stresses can be reliably used in design. The engineer further needs to know if, instead, key stresses are diverging because of singularities present. Then these stresses can be of no direct use in design. This paper describes some straightforward checks for assessing convergence or divergence of stresses from FEA.

The performance of the convergence-divergence checks suggested here is evaluated analytically with a simple error model, and with series analogues. These checks are also evaluated on an extensive set of diverging trial problems and converging test problems. Some alternative checks put forward elsewhere are likewise evaluated.

The evaluation of the suggested convergence-divergence checks shows that they can fairly consistently discern correctly whether stresses from FEA are converging or diverging. In addition, if converging, the evaluation shows that these checks can reasonably accurately and typically conservatively gauge the degree to which stresses have actually converged. In contrast, the evaluation shows that the alternative checks can conclude stresses are converging when, in fact, they are diverging. Thus these alternative checks can be seriously misleading.

## Introduction

### ***Background and motivation***

Inherent in determining stresses with finite element analysis (FEA) is discretization error. Only when discretization error is controlled is it possible to obtain sufficiently accurate stresses for comparison with strengths in designing for structural integrity. Needed therefore are *convergence* checks to control discretization error.

Comparably important for stresses from FEA is to know if, in actuality, they are diverging because of the presence of stress singularities. Then stresses cannot be meaningfully compared with strengths in designing for structural integrity. Needed therefore are *divergence* checks to ascertain when a stress singularity is present.

One example of the importance of convergence-divergence checks in the FEA of stresses comes from the jet engine industry. This example concerns the attachment of blades to disks in jet engines. Shown in Figure 1 is a section of a blade base and a segment of a disk to which it is attached. As a result of disk rotation, the blade wants to move vertically upwards (indicated by the arrow in Figure 1), and this tendency is restrained by contact with the disk (on  $CC'$  in Figure 1 after the gap closes). The particular detail in Figure 1 reflects the teaching of U.S. Patent 5,141,401 (Reference 1), which claims that FEA shows the contact stresses between the blade and the disk (on  $CC'$ ) are reduced as a result of undercutting the disk by an angle  $\phi$  (just above  $C$ ). In fact, with the undercut, local stresses  $\sigma$  are infinite as in

$$\sigma = \frac{E\phi}{2(1-\nu^2)(2\pi-\phi)} \ln r \quad \text{as } r \rightarrow 0 \quad (1)$$

where  $r$  is a dimensionless radial distance from the undercut vertex (Figure 1), and  $E$ ,  $\nu$  are Young's modulus, Poisson's ratio (taken as common for the blade and the disk). Stress singularities of this type are identified by Sneddon (Reference 2, Section 48.4): Fields for the specific configuration of Figure 1 can readily be assembled using fields in Reference 3, on page 282. Clearly, then, the stress-based reason put forward for the advantage of undercutting in Reference 1 is incorrect. Given effective convergence-divergence checks, such errors could and should be avoided.

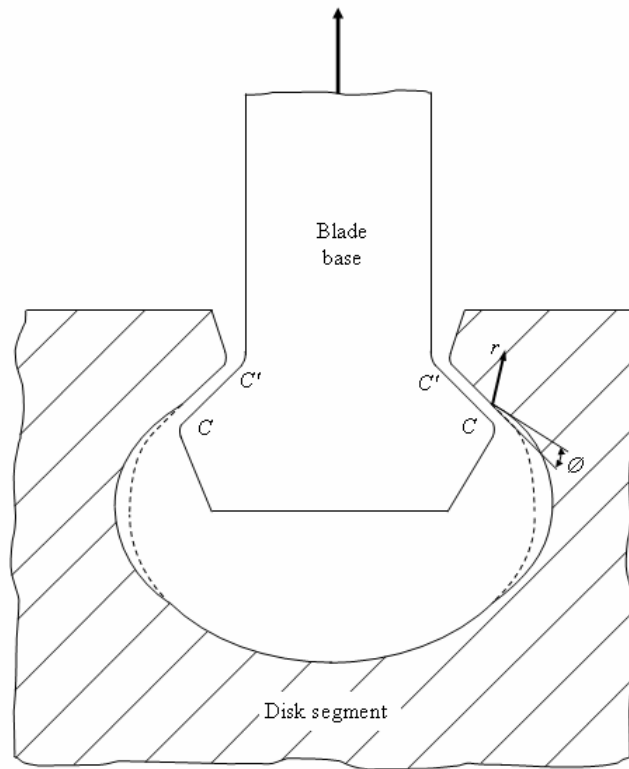


**Figure 1. Dovetail blade attachment with undercutting**

Unfortunately the foregoing example of a singular configuration in elastic stress analysis is far from a rare occurrence: Reference 4 furnishes a recent review of the asymptotic identification of stress singularities in 2D and 3D elasticity and underscores their abundant occurrence. Furthermore, while recourse to the references in Reference 4 can aid in the detection of stress singularities, there remains the possibility that the configuration for FEA has a singularity that is yet to be identified asymptotically. In general, then, effective convergence-divergence checks are essential for meaningful stresses from FEA.

### ***Literature review***

The last dozen years or so has seen an extensive amount of research on convergence of FEA for answers in general, and for stresses in particular. For the most part, this activity is well reflected in recent finite element texts: Akin (Reference 5, 2005), Cook *et al.* (Reference 6, 2002), Reddy (Reference 7, 2006), and Zienkiewicz *et al.* (Reference 8, 2005). All of these references discuss convergence of discretization error with mesh refinement. Most of this discussion centers on rates of convergence: Reference 6 provides an especially good discussion of this aspect of convergence. There are some implicit convergence checks for test problems in these texts. However, there are no explicit convergence checks for key stresses in applications in any of these texts. Too, while References 6 and 8 do discuss convergence in the presence of a stress singularity, there are no explicit divergence checks in any of these texts. These two omissions in

these texts reflect the dearth in the literature at large of explicit convergence-divergence checks for finite element stress analysis of applications.

Convergence checks in practice consist of two parts: an assessment of whether the FEA is *converging*, then, if it is, an assessment of whether it has *converged*. That is, is the FEA moving in the direction of the true key stresses sought with mesh refinement, then, if it is, has it got close enough? The latter assessment requires an estimate of the ultimate error in the key stresses sought. That is, a local *a posteriori* error estimate for the finest mesh used.

All of References 5-8 give considerable attention to discretization error and furnish explicit *a posteriori* error measures. These measures are global in nature (e.g., Zienkiewicz and Zhu, References 9,10). Such error measures can be effective in guiding element size gradation within a mesh so that accurate calculations of peak local stresses result (e.g., as in Reference 11). However, they cannot be used directly to estimate error in local stresses accurately. On the one hand, this is because an FEA of a specific nonsingular configuration can have different local stresses converge at different effective rates, so no one global error measure can capture these distinct errors. On the other hand, this is because an FEA of a specific singular configuration can have a local stress of interest diverge while a global error measure converges. Needed for local stresses are local error measures.

Of recent times, there has been more attention focused on local error measures rather than just global: A fairly recent review is given in Ainsworth and Oden (Reference 12, Chapter 8). In time, the results of this research can be expected to find their way into standard codes and assist stress analysts: For the present, their implementation typically requires development of additional computer algorithms used in concert with standard algorithms. Here, instead, we seek to provide simple local error measures that can be used with convergence tests using standard codes without any adjunct code.

### ***Outline of remainder of paper***

We begin with some simple suggestions for deciding if local stresses of interest are converging with mesh refinement; that is, are  $h$  convergent where  $h$  is a measure of element size. If judged converging, we offer a companion direct estimate of the extent to which local stresses have converged; that is, a local discretization-error estimate. If judged not converging, we offer some singularity signatures to gauge if the lack of convergence is because of a stress singularity, or because the FEA simply has yet to converge sufficiently. We also describe some alternative convergence checks that could take less computational effort to implement.

As a preliminary evaluation of the suggested checks, we next examine their performance with a simplified discretization-error model. This evaluation suggests some improvements with a view to being conservative.

As a first 1D evaluation of the improved suggested checks, we examine their analogous performance when used in series summation. As a second 2D evaluation, we examine performance on a series of singular trial problems and nonsingular test problems (some detailed results for these problems are appended). These problems have analytically known singularities and known exact solutions, respectively. Here, though, we treat them as if they were applications with unknown solutions in applying the improved convergence-divergence checks. Then we can draw on the known solutions to evaluate how well they actually work. We also submit the alternative checks to a like evaluation. We close with remarks on both the improved suggested checks and the alternatives in light of the results found.

## **Candidate convergence-divergence checks**

### ***Simple convergence checks***

In a test problem with a known exact solution, it is straightforward to assess convergence of an FEA. With a first coarse mesh and a second refined mesh, direct comparison with the exact result for the stress of interest reveals whether the error is reducing with mesh refinement; that is, whether the FEA is converging. Then comparison of the result for this stress from the refined mesh reveals whether the error is sufficiently low; that is, whether the FEA has converged.

In an application, however, the true answer for the stress of interest is sought but, of course, not known *a priori*. Under these circumstances, checking for converging requires at least two successively-refined meshes for a total of three meshes: a coarse (C), a medium (M), and a fine (F). Furthermore, the medium and fine meshes should not be the outcome of minor refinements if a reasonably stern test of converging is to result. To avoid this shortcoming, at the outset we systematically refine meshes throughout by scaling element lengths by a scale factor  $\lambda$  with

$$\lambda \approx 2 \tag{2}$$

For  $\lambda = 2$ , a sample sequence of meshes for a rectangular plate is illustrated in Figure 2. For a general  $\lambda$ , if  $h$  is a linear measure of representative element size in the originating coarse mesh, we have the following sequence of mesh sizes:

$$C - h, M - h/\lambda, F - h/\lambda^2 \tag{3}$$

This leads to numbers of elements for different dimensional problems as in Table 1.

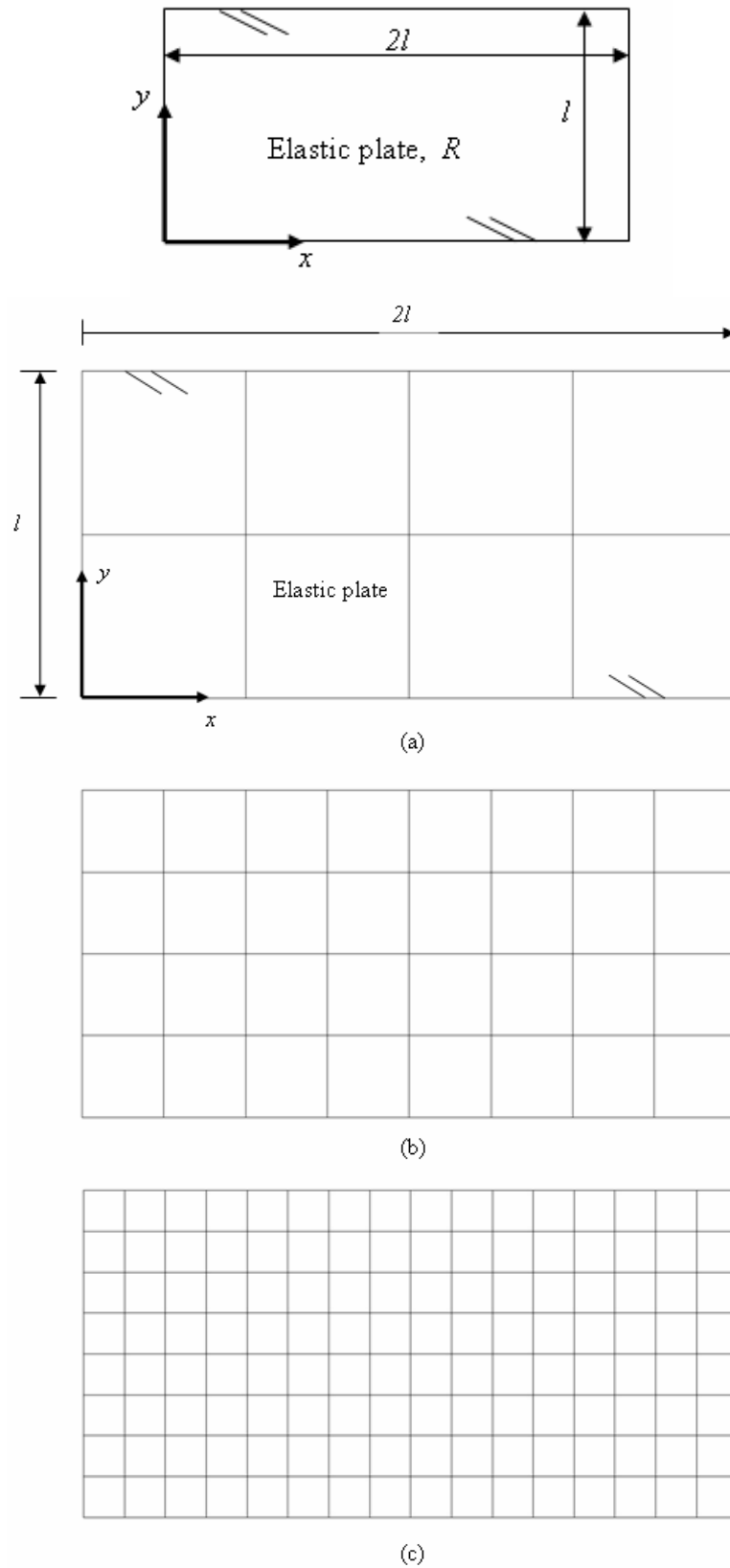


**Figure 2. Sample mesh refinement ( $\lambda = 2$ ) for a rectangular elastic plate (a) coordinates and coarse mesh, (b) medium mesh, (c) fine mesh**

**Table 1: Element numbers in mesh sequences for checks**

Mesh	1D	2D	3D
C	$N$	$N$	$N$
M	$\lambda N$	$\lambda^2 N$	$\lambda^3 N$
F	$\lambda^2 N$	$\lambda^4 N$	$\lambda^6 N$

On such mesh sequences, we initially adopt the following convergence checks. We judge the stress FEA to be *converging* if

$$|\sigma_m - \sigma_c| > |\sigma_f - \sigma_m| \quad (4)$$

provided  $(\sigma_c - \sigma_m)^2 + (\sigma_m - \sigma_f)^2 \neq 0$ , where  $\sigma$  is the stress of interest and subscripts distinguish the mesh used to calculate it (if  $\sigma_c = \sigma_m = \sigma_f$ , we judge the result to not only be converging, but also have converged)<sup>1</sup>. Given compliance with (4), we judge the stress FEA to have *converged* if

$$|\sigma_f - \sigma_m| / |\sigma_f| < \bar{\epsilon}_s \quad (5)$$

provided  $\sigma_f \neq 0$ , where  $\bar{\epsilon}_s$  is the relative error level sought. In practice, usually  $\bar{\epsilon}_s$  less than 0.01 (1%) serves as an excellent level, less than 0.05 (5%) as a good level, and less than 0.1 (10%) as a satisfactory level, though certainly more stringent levels can be set.

We have used convergence checks of this ilk for some time (e.g., Reference 13, 1982), though only relatively recently explicitly stated them (Reference 14, 1999). We make no claim of originality, either for Reference 14 or the present paper. It seems certain that other finite element users have employed similar, if not completely equivalent, checks in applications (though, to date, we have not found an explicit statement of such checks).

Before turning to divergence, it is important to set expectations re the likely success of the convergence checks in (4), (5). No such checks can rigorously be guaranteed to predict convergence when it truly occurs. More importantly, conversely no such checks can rigorously be guaranteed to predict divergence when it truly occurs. Given, therefore, some element of judgment is involved, caution is appropriate to try and realize conservativeness in practice. That is, to avoid predicting convergence when in fact key stresses from the FEA are diverging.

With this caveat in mind, we adjoin the following additional requirement for converging to (4):

$$(\sigma_m - \sigma_c)(\sigma_f - \sigma_m) > 0 \quad (6)$$

unless  $\sigma_m = \sigma_f$  (if  $\sigma_m = \sigma_f$ , we judge the result to be converging and converged). When (4) holds but (6) does not, further meshes are to be run to decide if FEA stresses are converging. This added condition removes oscillatory convergence from consideration, a response for which it is difficult to estimate discretization errors in FEA stresses directly. It also reduces the probability of predicting convergence when in fact stresses are oscillatory and diverging, as on rare occasions they can be in elasticity.

---

<sup>1</sup> One might think that  $\sigma_f$  could simply play the role of the exact solution and take  $|\sigma_f - \sigma_c| > |\sigma_f - \sigma_m|$  as a converging check instead of (4): Such a check fails to detect the presence of stress singularities.

## Singularity signatures

When (6) is complied with but (4) is not, we have two possibilities: the FEA is not yet apparently converging/converged on the mesh sequence at hand, or the FEA is diverging. The former occurs when the fine mesh result for the stress of interest is still a long way from the true result because of the coarseness of even this mesh. The latter occurs when stress singularities are present. Being able to distinguish which circumstance is applicable is useful because it determines whether more refined FEA is useful, as in the former case, or useless, as in the latter case. The most reliable means of distinction is via asymptotic identification of stress singularities (see Reference 4 for a recent review). Absent asymptotics, we use the following singularity signatures to determine their presence.

Stress singularities occur in two predominant forms in elasticity: power singularities and logarithmic singularities. For power singularities, the local stress  $\sigma$  behaves like

$$\sigma = O(\sigma_0 r^{-\gamma}) \quad \text{as } r \rightarrow 0 \quad (7)$$

wherein  $\sigma_0$  is an applied stress,  $r$  is a dimensionless radial distance from the singular point, and  $\gamma$  is the singularity exponent. For logarithmic singularities,  $\sigma$  behaves like<sup>2</sup>

$$\sigma = O(\sigma_0 \ln r) \quad \text{as } r \rightarrow 0 \quad (8)$$

With local FEA values of  $\sigma$  being typically extrapolated from nearby points in the elements adjoining the singular point, and these elements being refined as in (3), the following singularity signatures result: for *power singularities*

$$\frac{\sigma_m}{\sigma_c} \sim \frac{\sigma_f}{\sigma_m} \sim \lambda^\gamma \quad \text{as } h \rightarrow 0 \quad (9)$$

and for *log singularities*

$$\sigma_c - \sigma_m \sim \sigma_m - \sigma_f \sim \sigma_0 \ln \lambda \quad \text{as } h \rightarrow 0 \quad (10)$$

The result in (10) is the underlying reason for the strictly greater than sign in condition (4) for converging. To implement the asymptotic results in (9) and (10), we proceed as follows.

For power singularities, we obtain successive estimates of the singularity exponent via

$$\hat{\gamma} = [\ln(\sigma_m/\sigma_c)]/\ln \lambda, \quad \tilde{\gamma} = [\ln(\sigma_f/\sigma_m)]/\ln \lambda \quad (11)$$

provided  $\sigma_c, \sigma_m$  and  $\sigma_f$  are all of the same sign and  $\sigma_c \neq 0$ . Then we judge exponent estimates to be constant and a *power singularity present* if

$$\frac{2|\hat{\gamma} - \tilde{\gamma}|}{\hat{\gamma} + \tilde{\gamma}} < 0.1 \quad (12)$$

That is, the change in exponent is less than 10% of its average value. This percentage is provisional: Ultimately we need to validate it on numerical experiments. Given validation, then we judge there to be no power singularity if (12) does not hold.

For logarithmic singularities, we obtain successive estimates of the increment in the stress when (6) holds via

$$\Delta\sigma_c = \sigma_m - \sigma_c, \quad \Delta\sigma_m = \sigma_f - \sigma_m \quad (13)$$

Then we judge increments to be constant and a *log singularity present* if

---

<sup>2</sup> In (1),  $\sigma_0$  effectively is  $E\phi/[2(1-\nu^2)(2\pi-\phi)]$ .

$$\frac{2|\Delta\sigma_c - \Delta\sigma_m|}{|\Delta\sigma_c + \Delta\sigma_m|} < 0.1 \quad (14)$$

That is, the same provisional percentage change as for (12). In effect, (14) sets the range for which numerical equality is judged to hold between the terms on either side of (4), and an FEA is deemed to be diverging because of a log singularity. If neither (12) nor (14) hold when (4) does not hold, we judge the FEA to be not yet apparently converging/converged, henceforth termed nonconvergent.

Typically with stress singularities, other contributions to the stress at the singular point are  $o(1)$  as  $r \rightarrow 0$ . On occasion, however, stress singularities occur in concert with a hydrostatic pressure that can mask their presence. When this is the case, (13), (14) can still be used to identify log singularities, but (11), (12) require adaptation to be effective in identifying power singularities. If the magnitude of the hydrostatic pressure is known, it can simply be subtracted out and (11), (12) then used. If the magnitude is not known, (11) needs to be replaced by

$$\hat{\gamma} = \left[ \ln \left( \frac{\sigma_f - \sigma_m}{\sigma_m - \sigma_c} \right) \right] / \ln \lambda, \quad \tilde{\gamma} = \left[ \ln \left( \frac{\sigma_{f'} - \sigma_f}{\sigma_f - \sigma_m} \right) \right] / \ln \lambda \quad (15)$$

then (15), (12) used. In (15),  $\sigma_{f'}$  is  $\sigma$  calculated on a yet more refined mesh than the fine. For the occasional singular configuration, it is also possible for there to be a constant contribution to some but not all normal stress components which can mask the singular behavior in these components: Then simply considering other normal stresses helps reveal the singularities presence. Even with such adjustments, regular stresses can camouflage singular stresses to some extent. Accordingly we judge a singularity to occur if *any* stress component satisfies (12) or (14) at the location of the key stress of interest, and thus key stress values there to be unacceptable.

### **Alternative convergence-divergence checks**

When  $\lambda = 2$ , stern convergence checks result, but the numbers of elements in the fine mesh are  $4N$ ,  $16N$  and  $64N$  for 1D, 2D and 3D problems, respectively (see Table 1). With some planning when constructing the initial coarse mesh, and given today's computer capabilities, this should be feasible for 1D and 2D problems. However, for 3D it may prove to be too computationally taxing.

One means of reducing computational effort is to confine mesh refinement to the vicinity of where the stress of interest acts: We investigate this possibility further with our test problems. Another means is to use a smaller scale factor, but still one that results in a fairly stern convergence check. A choice of  $\lambda = 3/2$  would seem to be a reasonable compromise in this regard. Then element numbers for the mesh sequence of (3) are  $N$ ,  $3.4N$  and  $11.4N$  in 3D. If this still proves too taxing, a mesh sequence formed by first coarsening the coarse mesh then refining it may make computation feasible: that is, a sequence with  $0.3N$ ,  $N$  and  $3.4N$  in 3D.

Presumably also with a view to reducing computational effort, some alternative convergence-divergence checks are sometimes practiced in FEA. The first of these alternatives employs a mesh sequence with *linearly increasing* numbers of elements. Thus convergence-divergence checks on the mesh sequence

$$C - N, M - 2N, F - 3N \quad (16)$$

and so on. This sequence is used irrespective of the dimension of the problem, so 3D problems are more computationally tractable. Here we would use it in conjunction with (4), (5), (6) to try to gauge converging and converged, and (12), (14) to try to distinguish diverging from nonconverging.

Clearly as the sequence in (16) continues, we have diminishing changes in meshes to the point of being minor (e.g., ... $100N$ ,  $101N$ , ...). This makes it all too easy for (4), (5), (6) to be complied with when the FEA may be not converged, or worse, not converging. Thus such linearly increasing sequences have the potential of being nonconservative. However, possibly in practice at the outset, the sequence of (16) suffices and thereby reduces computation. We investigate this possibility subsequently.

The second of these alternatives employs just a *two-mesh* check. Here, then, convergence-divergence checks on the first two meshes of (3) using just the counterpart of (5) on C and M meshes to decide if

converged or not. This abbreviated sequence is used irrespective of the dimension of the problem, so potentially taxing computations for fine meshes in 3D are avoided.

This two-mesh approach would appear to be quite vulnerable to being nonconservative. With just two meshes, nonconservative estimates of final discretation error can easily result with oscillatory convergence, something not guarded against by (6) because it cannot be applied. Further, there is no assessment of converging. Consequently there is the increased possibility of judging an FEA to have converged, when in fact it is diverging because of a weak singularity with small, but not decreasing, stress increments. We investigate these concerns for two-mesh checks subsequently.

## Evaluation via an error model

### **Error model**

We define the *local discretization error*  $e$  for the stress of interest  $\sigma$  by

$$e = (\sigma_a - \sigma_h) \operatorname{sgn}(\sigma_a) \quad (17)$$

where  $\sigma_a$  is the actual or true value of  $\sigma$ ,  $\sigma_h$  the value as determined via FEA on a mesh of size  $h$ , and  $\operatorname{sgn}$  is the signum function. With this definition,  $e$  is positive whenever  $|\sigma_c| < |\sigma_m| < |\sigma_f| < |\sigma_a|$ . That is, whenever  $\sigma_a$  in magnitude is approached from below, the norm in FEA. Then we adopt the following *simplified model* for  $e$ :

$$e = e_0 (h/h_0)^c \quad (18)$$

wherein  $e_0$  is the value of  $e$  on an initial mesh of size  $h_0$ , and  $c$  is the *effective convergence rate* ( $c > 0$  for convergence).

Asymptotically as  $h \rightarrow 0$ , values of  $c$  are known (see, e.g., Cook *et al.*, Reference 6, Chapters 4, 9). For example, for a four-node quadrilateral element in plane elasticity, typically  $c \sim 1$ . This is so provided the problem for FEA is sufficiently continuous. Then  $c$  can even be increased, using superconvergent recovery techniques, to  $c \sim 2$  (see Zienkiewicz *et al.*, Reference 8, Chapter 13). However, even asymptotically,  $c$  is reduced absent sufficient continuity. For example, for conforming elastic contact problems,  $c \sim 1/2$  near the edge of contact once contact extent is established, and for a stress-free proud corner subtending an angle of  $150^\circ$  in an elastic solid,  $c \sim 1/5, 0.534$ , in the vicinity of the corner for states of antiplane shear, plane strain, respectively (from, e.g., Reference 4, Sections 4.1, 2.1). Moreover, these three lower rates apply to higher-order elements such as the eight-node quadrilateral when used on the given examples, despite the fact that typically  $c \sim 2$  for eight-node elements. In general, then, quite a range of asymptotic convergence rates can result in the FEA of stresses.

Such variations are compounded for the effective convergence rate,  $c$ , of the simplified error model of (18). This model approximates actual power series in  $h$  for  $e$  with but one term. With  $h$  sufficiently small, the effective  $c$  of (18) does approach asymptotic values. However, for  $h$  as used in practice,  $c$  of (18) can differ appreciably from asymptotic values. For example, if  $c$  has two contributions of  $O(h)$  and  $O(h^2)$  of the same sign,  $c$  can be close to 2 on a given three-mesh sequence, rather than its asymptotic value of 1. Further, if these two contributions are of opposite sign,  $c$  can be markedly less than 1 and even negative on a given three-mesh sequence. Hence, in practice, the determination of an effective convergence rate can be quite sensitive to the mesh size used.

### **Simple checks: Modified converged checks**

Despite the somewhat capricious nature of  $c$  in the simplified error model of (18), we apply this model to our mesh sequence of (3) with  $h$  therein replaced by  $h_0$ . Assuming  $\sigma_a > 0$  to aid the exposition, we thus have

$$\sigma_a - \sigma_c = e_0, \quad \sigma_a - \sigma_m = e_0 / \lambda^c, \quad \sigma_a - \sigma_f = e_0 / \lambda^{2c} \quad (19)$$

Eliminating  $\sigma_a$  by subtracting the second of (19) from the first and the third from the second, thereafter eliminating  $e_0$  by forming a quotient of the results, then taking logs, gives

$$c = \left( \ln \frac{\sigma_m - \sigma_c}{\sigma_f - \sigma_m} \right) / \ln \lambda \quad (20)$$

The same result holds for  $\sigma_a < 0$ . Under (6),  $c$  of (20) is guaranteed real. Further, convergence with  $c > 0$  occurs in (20) if and only if (4) holds. Hence a justification of our converging criterion when the simplified error model of (18) applies.

In effect in (5) we have an estimate of the absolute value of the relative discretization error  $\bar{e}$  where

$$\bar{e} = e / |\sigma_a| \quad (21)$$

Denoting this estimate by  $\hat{e}$ , we have

$$\hat{e} = |\sigma_f - \sigma_m| / |\sigma_f| \quad (22)$$

Now using the simplified error model of (18) and substituting in (21), (22) from (19) gives

$$\frac{\hat{e}}{|\bar{e}|} = \frac{|\lambda^c - 1|}{|1 - \bar{e}|} \quad (23)$$

provided  $\bar{e} \neq 1$ , where  $\bar{e}$  here is the relative discretization error for the fine mesh. If  $\lambda^c > 2$  and  $\bar{e} > 0$ , the ratio in (23) is greater than 1, and  $\hat{e}$  is a conservative estimate of  $|\bar{e}|$ .

To guard against  $\lambda^c < 2$ , and thereby  $\hat{e}$  leading to a nonconservative estimate, we adopt the modified estimate  $\tilde{e}$  where

$$\tilde{e} = \hat{e} / |\lambda^c - 1|, \quad \lambda^c < 2 \quad (24)$$

with  $c$  as estimated by (20). That is, if  $\lambda = 2$ , we use (24) instead of (22) when  $c < 1$ , and if  $\lambda = 3/2$ , when  $c < 1.71$ . Now, therefore, our converged check compares  $\hat{e}$  of (22) with  $\bar{e}_s$  when

$\lambda^c \geq 2$ ,  $\tilde{e}$  of (24) with  $\bar{e}_s$  when  $\lambda^c < 2$ . We use this modified converged check on low-order elements (four-node quadrilaterals, three-node triangles).

For second-order elements (eight-node quadrilaterals, six-node triangles), we try to take advantage of their potentially improved convergence rates in problems other than contact problems by taking, instead of (24),

$$\begin{aligned} \tilde{e} &= \hat{e} / |\lambda^c - 1|, \quad c \leq 2 \\ \tilde{e} &= \hat{e} / |\lambda^2 - 1|, \quad c > 2 \end{aligned} \quad (25)$$

with  $c$  continuing to be estimated by (20). The first of (25) includes (24). The second of (25) limits the degree to which we use estimated  $c$  to extrapolate error estimates.<sup>3</sup>

Even with these modifications, our converged check can still be nonconservative ( $\hat{e}$  or  $\tilde{e} < |\bar{e}|$ ). This can happen when  $\bar{e} < 0$  and peak stresses are approached from above (see (23)). While this is not the norm in FEA, it can happen. However, then we should at least be alerted to the possibility of a nonconservative error estimate by having  $|\sigma_c| > |\sigma_m| > |\sigma_f|$ . It can also happen when  $c$  of (20) overestimates the actual effective convergence rate. We can obtain an appreciation of how often this actually happens from our later numerical experiments.

---

<sup>3</sup> For yet higher-order elements, one could extend the range of applicability of the first of (25) to yet higher values of  $c$ . This possibility is not investigated here.

## **Alternative checks: Divergence detection?**

We also use the simplified error model of (18) to evaluate the alternative convergence-divergence checks, paying special attention to when these alternatives can be nonconservative.

For the linearly increasing mesh sequence of (16), the counterpart of (3) is

$$C - h, M - h/2^{i/i}, F - h/3^{i/i} \quad (26)$$

where  $i = 1, 2, 3$  for 1D, 2D, 3D, respectively, is the number of dimensions involved. Then applying (18) to the mesh sequence of (26) with  $h$  therein replaced by  $h_0$ , and proceeding as previously, yields

$$\frac{\sigma_m - \sigma_c}{\sigma_f - \sigma_m} = \frac{6^{c/i} - 3^{c/i}}{3^{c/i} - 2^{c/i}} \quad (27)$$

From (27) when (6) holds, we find our converging check (4) to be complied with when

$$c > -i \quad (28)$$

Clearly since  $c < 0$  corresponds to divergence, this alternative can be nonconservative: That is, predict convergence when in fact FEA stresses are diverging. Moreover, the higher the dimension of the problem being analyzed, the more likely such nonconservative predictions are to result.

For the two-mesh check, applying (18) to the counterpart of (22) gives

$$\hat{e} = \frac{|e_0(1 - 1/\lambda^c)|}{|\sigma_a(1 - \bar{e})|} \quad (29)$$

where  $\hat{e}$  and  $\bar{e}$  are the estimated and actual, relative, discretization errors for the medium mesh. Thus the two-mesh counterpart of (5) can be met if  $\lambda^c \rightarrow 1, c < 0$ , and FEA stresses are actually diverging, albeit slowly. Further, normalizing (29) by  $\bar{e}$  for the medium mesh leads to (23) except that now  $\hat{e}, \bar{e}$  are for the medium mesh. As for (23), this can be nonconservative whenever  $\lambda^c < 2$ . Now, though, absent a third mesh we do not have available an estimate of  $c$  as in (20) to help remedy the situation as in (24) or (25). Consequently this alternative can give nonconservative estimates of discretization errors. As pointed out earlier, it can also be nonconservative when (6) does not hold and we have oscillatory convergence.

## **Evaluation via a series analogy**

### **Series analogy and test series**

As a 1D analogy, we recall classical series summation. We denote partial sums  $S_N$  of the sequence  $\{a_n\}$  by

$$S_N = \sum_{n=1}^N a_n \quad (30)$$

Thus in our series analogy,  $N$  becomes the number of terms in the sum instead of the number of elements. To aid the exposition, we take  $a_n > 0$ . Hence  $S_N$  is absolutely convergent if the limit  $N \rightarrow \infty$  is bounded.

A necessary condition for  $S_N$  to be so convergent is that

$$\lim_{n \rightarrow \infty} a_n = 0 \quad (31)$$

Further, from d'Alembert's ratio test,

$$\lim_{n \rightarrow \infty} \frac{a_{n+1}}{a_n} < 1 \Rightarrow \text{convergent series} \quad (32)$$

$$\lim_{n \rightarrow \infty} \frac{a_{n+1}}{a_n} > 1 \Rightarrow \text{divergent series}$$

This test fails if the ratio equals 1.

We now view the value of stress of interest,  $\sigma$ , as the outcome of a sequence of FEA determinations summed in accordance with

$$\sigma = \sigma_c + (\sigma_m - \sigma_c) + (\sigma_f - \sigma_m) + \dots \quad (33)$$

To interpret these successive terms as  $a_n$  in (30) with  $a_n > 0$ , we assume  $0 < \sigma_c < \sigma_m < \sigma_f < \sigma_a$ . Then our converging check (4) under (6) is analogous to the ratio test of (32), except that we do make a determination of divergence when the ratio is 1, and our converged test is analogous to the necessary condition of (31).

To explore this analogy further, we seek to apply our checks of (4), (5), and (6), as well as (12), (14), (22), (24) and (25), to a set of series which are independently known either to be convergent or divergent, and see how well our checks predict this behavior. A first candidate pair of series to this end are the classical arithmetic progression (AP) and geometric progression (GP):

$$\begin{aligned} a_n &= n, S_N = N(N+1)/2 \\ a_n &= \alpha^n, S_N = \alpha(1-\alpha^N)/(1-\alpha) \end{aligned} \quad (34)$$

where  $\alpha$  is a constant. The GP of (34) is convergent if  $\alpha < 1$ , divergent otherwise, while the AP is simply divergent. Some other series that can be used in this way are given in Table 2, together with asymptotic values as  $N \rightarrow \infty$  from integral estimates,  $\tilde{S}_N$ . In  $\tilde{S}_N$ ,  $C_1 = 1.459$ ,  $C_2 = 2.613$ , and  $\Gamma$  is Euler's constant: These asymptotic values apply for  $N \geq 4$  and are actually accurate to within 0.1% for all such  $N$ . The first of the series in Table 2 diverges as  $\sqrt{N}$ , and so is like a power singularity: The second diverges as  $\ln N$ , and so is like a log singularity. The remaining series are convergent with slow convergence akin to a contact problem, linear convergence as can occur in a regular problem with low-order elements, and rapid convergence as can be the case with high-order elements.

**Table 2: Test series**

$a_n$	$\tilde{S}_N$	$R$
$\frac{1}{pn}$	$2\sqrt{(N+\frac{1}{2})} - C_1$	$\sqrt{2}$
$\frac{1}{n}$	$\ln(N+\frac{1}{2}) + \Gamma$	1
$\frac{1}{n^{3/2}}$	$C_2 - \frac{2}{p(N+\frac{1}{2})}$	$\frac{1}{p2}$
$\frac{1}{n^2}$	$\frac{\pi^2}{6} - \frac{1}{N+\frac{1}{2}}$	$\frac{1}{2}$
$\frac{1}{n^4}$	$\frac{\pi^4}{90} - \frac{1}{3(N+\frac{1}{2})^3}$	$\frac{1}{8}$

### Simple checks with modifications

Because all  $a_n > 0$ , (6) is automatically complied with. To check (4), we form the ratio

$$R = \frac{S_{4N} - S_{2N}}{S_{2N} - S_N} \quad (35)$$

Then (4) for  $\lambda = 2$ , in effect, has the series converging if  $R < 1$ , diverging or nonconvergent if  $R \geq 1$ .

From (34) for the AP,  $R \sim 4 > 1$  as  $N \rightarrow \infty$ , so (4) correctly predicts not converging for large  $N$ . In fact,  $R > 1$  for all  $N$ , so that this correct prediction holds for any  $N$ . Further, (12) holds for  $N \geq 2$  and  $\gamma \sim 2$ .

This series, therefore, could be interpreted as equivalent to the power singularity associated with a concentrated moment. Irrespective of how appropriate such an interpretation is, (12) certainly predicts that the series is divergent rather than just nonconvergent.

From (34) for the GP,

$$R = \alpha^N (1 + \alpha^N) \quad (36)$$

Hence (4) predicts the series is convergent if

$$\alpha < \left( \frac{2}{1 + \sqrt{5}} \right)^{1/N} \quad (37)$$

While (37) is true, it is conservative: In reality, the GP is convergent for any  $\alpha < 1$ .

For the other series of Table 2, the asymptotic values of  $R$  of (35) given in this table show that (4) predicts the first two to be not converging and the last three to be converging, as is indeed the case. Moreover (4) does this for all  $N \geq 1$ , not just  $N \rightarrow \infty$ .

For  $a_n = 1/n^{1/2}$ , (12) is complied with for  $N \geq 1$ , so divergence analogous to a power singularity (with  $\gamma \sim 1/2$ ) is predicted rather than just a nonconvergent series. For  $a_n = 1/n$ , (14) is complied for  $N \geq 2$ , so divergence analogous to a log singularity is predicted rather than just a nonconvergent series. Given the asymptotic expressions  $\tilde{S}_N$  in Table 2, both of these predictions would seem to be appropriate.

For  $a_n = 1/n^{3/2}$ , the analogue of (22) with  $\lambda = 2$  has

$$\hat{e} \sim \frac{p^2 - 1}{C_2 p N} \quad \text{as } N \rightarrow \infty \quad (38)$$

In fact

$$\bar{e} \sim \frac{1}{C_2 p N} \quad \text{as } N \rightarrow \infty \quad (39)$$

so  $\hat{e}$  is nonconservative. Now, though, (20) gives  $c \sim 1/2$ , so our modified estimate of (24) applies. This gives

$$\tilde{e} \sim \frac{1}{C_2 p N} \quad \text{as } N \rightarrow \infty \quad (40)$$

Hence an asymptotically correct estimate and support for our adoption of the modified error estimate of (24) when convergence is slow.

For  $a_n = 1/n^2$ , we have, from the analogues of (22), (21),

$$\hat{e} \sim \bar{e} \sim \frac{3}{2\pi^2 N} \quad \text{as } N \rightarrow \infty \quad (41)$$

Hence an asymptotically correct error estimate. Here (20) gives  $c \sim 1$ , so with  $\lambda = 2$  there is no need to apply (24).

For  $a_n = 1/n^4$ , we have

$$\hat{e} \sim \frac{105}{32\pi^4 N^3}, \quad \bar{e} \sim \frac{15}{32\pi^4 N^3} \quad \text{as } N \rightarrow \infty \quad (42)$$

Hence a conservative estimate by a factor of 7. Now, though, (20) gives  $c \sim 3$ , so applying (25) we have

$$\tilde{e} \sim \frac{35}{32\pi^4 N^3} \quad \text{as } N \rightarrow \infty \quad (43)$$

Hence still a conservative estimate but a more accurate one.

Thus applying our convergence-divergence checks correctly predicts divergence whenever series actually diverge. Further, these checks typically predict convergence whenever series actually converge, the exception being for some convergent GP for which they predict not converging. Companion error estimates, modified where appropriate, are asymptotically accurate, or if not, at least conservative. All told, a satisfactory and conservative performance by these checks.

### **Alternative checks: Divergence detection?**

For the first alternative with linearly increasing numbers of elements, the analogue of (4) has series converging when  $a_n > 0$  if

$$a_{N+1} = S_{N+1} - S_N > S_{N+2} - S_{N+1} = a_{N+2} \quad (44)$$

That is, requiring  $a_n$  be decreasing in magnitude, as in (31). While (31) is a necessary condition for convergence, it is not sufficient. Accordingly, although (44) can predict convergence when series are indeed convergent, it can also predict convergence when series are divergent. An example of the former is the GP; for this series, (44) correctly predicts convergence when  $\alpha < 1$ . An example of the latter is the harmonic progression of Table 2,  $a_n = 1/n$ ; for this series, (44) incorrectly predicts convergence when, in fact, the series is divergent. A further example is  $a_n = 1/n^{1/2}$  where again (44) predicts convergence when

the series is divergent. As with the previous error model evaluation, therefore, this alternative check exhibits an inability to detect divergence. Such an inability represents a serious nonconservative failure for this alternative check.

For the second alternative with a two-mesh check, the analogue for series would have the series being satisfactorily summed ( $\bar{\epsilon}_s < 0.1$ ) when  $a_n > 0$  if

$$(S_{2N} - S_N)/S_{2N} < 0.1 \quad (45)$$

For the AP, (45) is never complied with so that this series would never be regarded as summed. However, for the harmonic progression

$$(S_{2N} - S_N)/S_{2N} \sim (\ln 2)/(\ln N) \quad \text{as } N \rightarrow \infty \quad (46)$$

Hence for  $N > 1024$ , (45) is met, and the series is predicted to be satisfactorily summed when, in fact, it is divergent. For still larger  $N$ , (46) with a two-mesh check could even indicate summation to within an excellent error level. Analogously to the previous error model evaluation, therefore, this alternative check exhibits an inability to reject diverging results. Such an inability represents a serious nonconservative failure for this alternative check.

## Numerical experiments: Diverging stresses with power singularities

### *Simple checks with modifications*

Here we apply our simple convergence-divergence checks, modified when appropriate, to see if they can detect divergence on a set of trial problems with power singularities. These are ‘trial’ problems rather than true test problems because they do not have known exact solutions throughout the elastic solid for analysis: However, these trial problems do have known, asymptotically-identified, stress singularities at a point in the elastic solid, and this level of analytical knowledge suffices for the present assessment.

These singular trial problems are for: bimaterial reentrant corners under tension, butt joints under tension, reentrant corners under tension and both in-plane and out-of-plane shear, and elastic half-spaces indented by rigid flat-ended punches. All told, 14 different problems with known power singularities.

A variety of 2D ANSYS elements are used in the analysis of these singular trial problems: four-node quadrilaterals (4Q, PLANE42 of Reference 15), eight-node quadrilaterals (8Q, PLANE82 of Reference 15), six-node triangles (6T, PLANE2 of Reference 15), and three-node triangles (3T, triangle option in PLANE42 of Reference 15). This variety is employed to assess the robustness of our convergence-divergence checks with respect to element choice. Typically these elements are run in the plane strain mode, the axisymmetric mode only being used for one contact problem. Given the general asymptotic equivalence of plane strain and axisymmetric singular stresses in elasticity (Zak, Reference 16), we do not expect much difference between the FEA of these two states; This axisymmetric, singular, contact problem is merely run to confirm this expectation by comparison with its plane strain counterpart.

For the bimaterial corners, free meshes with nearly uniformly-sized elements are used (AMESH, Reference 15). For the other problems, uniform structured meshes are used. All problems are analyzed on at least three meshes with systematic refinement as in (3) with  $\lambda = 2$  (see References 17-20 for details).

There are, of course, superior approaches to the FEA of singular stress problems given one acts on an awareness of a stress singularity’s presence at the outset. Then for inverse-square-root singularities, there are quarter-point elements (Henshell and Shaw, Reference 21; Barsoum, Reference 22), and for other singularities, other mid-side node placements (Wait, Reference 23). Alternatively, elements adjoining the singular point can be enriched with analytical expressions reflecting asymptotic singular character, or, at the very least, element sizes can be significantly reduced in the vicinity of the singularity to capture it better. All such approaches would presumably then seek to determine the coefficient of the stress singularity, rather than the singular, and thus locally infinite, stress itself (see Reference 24 for a fairly recent review of various means of extracting singularity coefficients). With such coefficients accurately determined, it might then be possible to use them in a generalized fracture mechanics treatment.

This is *not* what we are doing here. Instead we are proceeding as if we had no awareness of the stress singularity's presence and asking our convergence-divergence checks to reveal its presence. Hence the use of unbiased uniform or nearly uniform meshes to provide a fair assessment of the effectiveness of our convergence-divergence checks in this regard.

A total of 60 such meshes are run on the trial problems with power singularities to assess the ability of our convergence-divergence checks to detect FEA divergence. Viewing one three-mesh sequence as a single numerical experiment, these meshes give rise to 26 experiments. Here we present some selected results, then merely summarize the performance of our convergence-divergence checks re divergence detection (companion detailed results are set out in Appendix A).

As a first selected example, we consider an elastic bimaterial plate with a right-angled reentrant corner under tension (Figure 3,  $\phi = 90^\circ$ ). In addition to boundary conditions applying a normal transverse traction  $\sigma_0$ , the plate has stress-free conditions on the corner flanks and symmetry conditions on the boundary at  $x = l$  (Figure 3). The upper and lower halves are perfectly bonded on  $y = 0$  (Figure 3). The halves have a common Poisson's ratio of  $1/4$ , but distinct Young's moduli of  $E_+, E_-$  for  $y > 0, y < 0$ , respectively. Here we consider  $E_+/E_- = 16$ . From Bogy (Reference 25), this choice may be shown to lead to two singularities:

$$\sigma_s = O\left(\sigma_0\left(\frac{l}{r}\right)^{0.374}\right) + O\left(\sigma_0\left(\frac{l}{r}\right)^{0.218}\right) \text{ as } r \rightarrow 0 \quad (47)$$

where  $\sigma_s$  is any singular stress component at the singular point, and  $r$  is now as in Figure 3. With mesh refinement, then, we can expect the stronger singularity to dominate and  $\hat{\gamma}, \tilde{\gamma}$  of (11) to approach 0.374 with (12) holding: It remains to be seen how true this is for actual FEA results, especially given the presence of a second singularity.

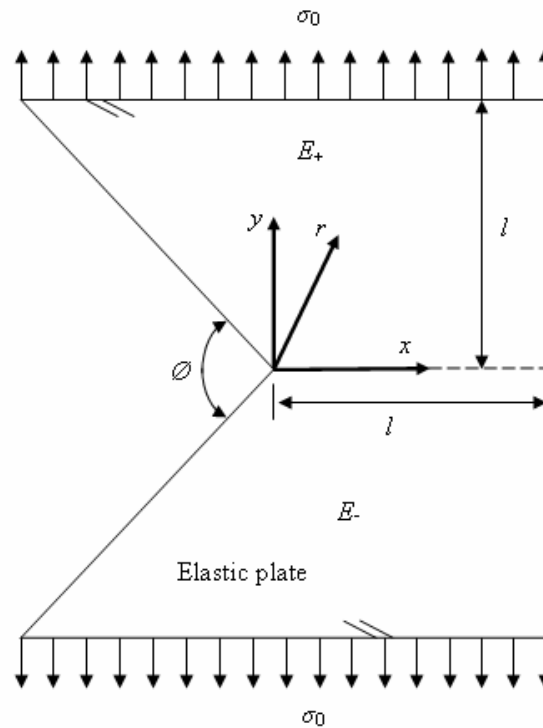


**Figure 3. Bimaterial elastic plate with a reentrant corner under tension**

The FEA of this bimaterial configuration uses free meshes of 6T elements (see Reference 17 for further specifics). We thus have results as in Table 3 for the maximum normalized stress

$$\bar{\sigma}_{\max} = \sigma_y (\text{at } x = y = 0) / \sigma_0 \quad (48)$$

where coordinates are as in Figure 3. Like results for other corners are given in Appendix A, Table 15.

**Table 3: Divergence detection for a bimaterial corner under tension ( $E_+/E_- = 16$ )**

$m$	$\bar{\sigma}_{\max}$	$\Delta \bar{\sigma}_{\max}$	$\hat{\gamma}, \tilde{\gamma}$
1	8.82		
		2.74	0.390
4	11.56		
		3.55	0.386
16	15.11		

In Table 3, the mesh number,  $m$ , reflects the number of elements used. Specifically

$$N_m = mN_1 \quad (49)$$

where  $N_1 = 128$  is the number of elements in mesh 1, the initial coarse mesh, and  $N_m$  the number in mesh  $m$ . Hence for the  $m$  of Table 3, refinement as in (3) with  $\lambda = 2$ . Further,  $\Delta \bar{\sigma}_{\max}$  is the difference between  $\bar{\sigma}_{\max}$  on successive meshes, hence the counterpart of the differences in (4).

Clearly in Table 3, (6) is complied with but (4) is not, so our convergence-divergence checks do not predict convergence. Then (11) has successive exponent estimates as in Table 3, yielding

$$\frac{2|\hat{\gamma} - \tilde{\gamma}|}{\hat{\gamma} + \tilde{\gamma}} = 0.01 \quad (50)$$

in compliance with (12), so our convergence-divergence checks correctly predict the presence of a power singularity. Moreover, despite the presence of a second singularity of weaker yet comparable strength, the singularity exponent ultimately estimated is close to the actual exponent (3% higher, see (47)).

This first example is for a strong singularity. A sterner test of our convergence-divergence checks results if we have a weaker power singularity. Accordingly, as a second selected example, we consider an elastic bimaterial plate with a butt joint under tension (Figure 4). Aside from the application of  $\sigma_0$ , the plate is stress free on its edges. The adherend (Young's modulus  $E_+$ ) and adhesive ( $E_-$ ) are perfectly bonded on their interface at  $y = l/20$  (Figure 4). The adherend and adhesive have a common Poisson's ratio of  $1/3$ , but distinct Young's moduli with  $E_+/E_- = 2$ . Absent a reentrant corner and with a smaller material discontinuity, this configuration should be less singular than our first: Indeed, this is the case. From Bogy (Reference 26), we now have

$$\sigma_s = O\left(\sigma_0 \left(\frac{l}{r}\right)^{0.042}\right) \text{ as } r \rightarrow 0 \quad (51)$$

where  $r$  is as in Figure 4.

The FEA of this bimaterial configuration uses structured uniform meshes of 4Q elements. The initial coarse mesh has  $N_1 = 110$  on  $R$  via symmetry (see Figure 4). Subsequent meshes have

$$N_m = 2^{2(m-1)} N_1 \quad (52)$$

elements,  $m = 2-5$  being the mesh number for this analysis. Thus meshes in compliance with (3) for  $\lambda = 2$ . Results for this particular butt joint are as in Table 4 wherein now

$$\bar{\sigma}_{\max} = \sigma_y \text{ (at } x = l, y = l/20) / \sigma_0 \quad (53)$$

with coordinates as in Figure 4. Like results for a butt joint with a stronger singularity are given in Appendix A, Table 15.

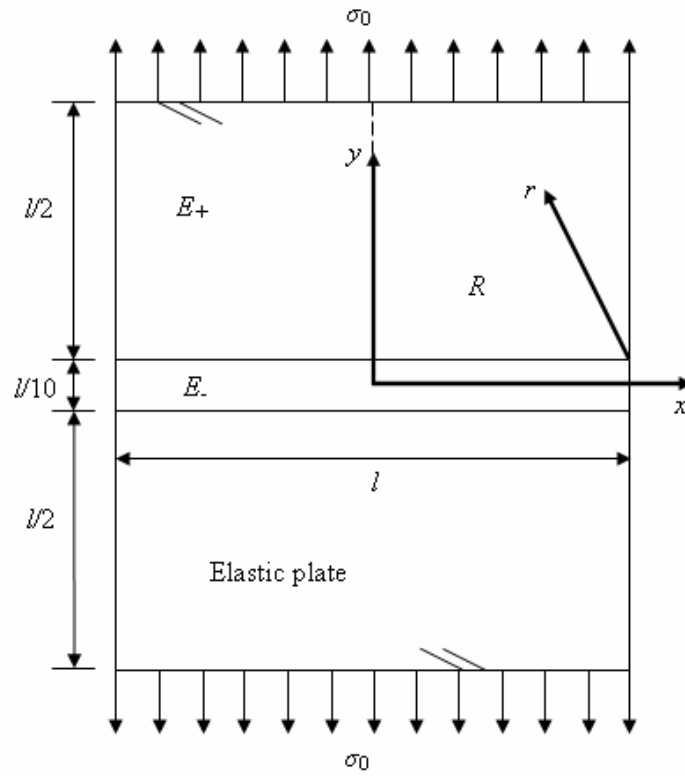


**Figure 4. Butt joint between elastic plates under tension**

**Table 4: Divergence detection for a butt joint under tension ( $E_+/E_- = 2$ )**

$m$	$\bar{\sigma}_{\max}$	$\Delta\bar{\sigma}_{\max}$	$\hat{\gamma}, \tilde{\gamma}$
1	1.0326		
		0.0180	0.025
2	1.0506		
		0.0231	0.031
3	1.0737		
		0.0270	0.036
4	1.1007		
		0.0299	0.039
5	1.1306		

Clearly in Table 4, again (6) is complied with but (4) is not, so our convergence-divergence checks do not predict convergence. Then (11) has successive exponents as in Table 4. Using these pairwise for meshes 1, 2 and 2, 3, then 2, 3 and 3, 4, and finally for 3, 4 and 4, 5, there results the following values for the quotient of (12):

$$\frac{2|\hat{\gamma} - \tilde{\gamma}|}{\hat{\gamma} + \tilde{\gamma}} = 0.21, 0.15, 0.08 \quad (54)$$

Hence on meshes 1-4, (12) is not complied with and our convergence-divergence checks have that the FEA does not, yet anyway, reveal a power singularity. While this represents a lack of resolution on the part of the checks on these results, noncompliance with (4) at least means that a stress analyst would not accept them as either converging or converged. On meshes 4, 5, (12) is complied with and our convergence-divergence checks correctly predict the presence of a power singularity. Again the singularity exponent ultimately estimated is quite close to the actual exponent (7% lower, see (51)).<sup>4</sup>

As a third and final selected example, we consider another weak power singularity. This concerns an elastic plate with a right-angled reentrant corner as in Figure 3 when  $\phi = 90^\circ$ , but now comprised of a single material and under a shear traction of magnitude  $\tau_0$  on the upper and lower edges. The corner flanks continue to be stress free and now a counterbalancing moment is supplied via constant normal tractions on the plate edge at  $x = l$ . Absent a material discontinuity and with shear loading, a weaker singularity than in (47) should result: Indeed this is the case. From Williams (Reference 27), we now have

$$\sigma_s = O\left(\tau_0 \left(\frac{l}{r}\right)^{0.091}\right) \quad \text{as } r \rightarrow 0 \quad (55)$$

where  $r$  reverts to as in Figure 3.

<sup>4</sup> This particular configuration was also subjected to a subsequent submodel around the singular point. The submodel used 4Q elements and followed the procedure in Reference 11. It resulted in successive estimates of  $\gamma$  of 0.041, 0.042; hence a demonstration that our convergence-divergence checks can reveal power singularities with just local refinement.

The FEA of this reentrant corner configuration uses structured uniform meshes of 3T elements. The initial mesh has  $N_1 = 192$  and subsequent meshes have element numbers as in (52) (see Reference 18 for further specifics). Results for this particular corner are given in Table 5 wherein

$$\bar{\tau}_{\max} = \tau_{xy}(\text{at } x = y = 0) / \tau_0 \quad (56)$$

with coordinates as in Figure 3. Results for other reentrant corner configurations with stronger singularities are given in Appendix A, Table 17.

**Table 5: Divergence detection for a 90° reentrant corner under in-plane shear**

$m$	$\bar{\tau}_{\max}$	$\Delta \bar{\tau}_{\max}$	$c$	$\hat{\gamma}, \tilde{\gamma}$
1	3.594	0.402		
2	3.996	0.310	0.37	-
3	4.306	0.294	0.08	-
4	4.600	0.303	-	0.095
5	4.903			0.092

In Table 5, both (6) and (4) are complied on meshes 1-4, so our check has the maximum shear stress converging despite it being singular. However, calculating  $c$  from (20) results in the successive low values (<1) given in Table 5, whence successive error estimates from (24) of

$$\bar{\epsilon} = 0.25, 1.12 \quad (57)$$

Thus unsatisfactory error levels, and our modified convergence-divergence checks would at least not predict  $\bar{\tau}_{\max}$  had converged. In fact, on meshes 2, 3, 4, (14) is complied with and a log singularity predicted. While this is actually an errant prediction, it would certainly not see  $\bar{\tau}_{\max}$  being viewed as acceptable.

On the 3, 4, 5 mesh sequence, (6) is complied with but (4) is not, so  $\hat{\gamma}, \tilde{\gamma}$  values are calculated and included in Table 5. These values satisfy (12), the quotient therein being 0.03, so on these more refined meshes the weak power singularity present is detected. Again the singularity exponent ultimately estimated is quite close to the actual exponent (1% higher, see (55)).

It transpires that the results in Table 5 are the only ones that comply with (4) in the trial problems with power singularities. Thus (4) detects divergence or nonconvergence in 24/26 experiments (see Appendix A, Tables 15, 17, 18 for the additional results). Further, once (4) is not complied with, (12) indicates a power singularity in 23/24 experiments.<sup>5</sup> For the present set of numerical experiments, this performance is not significantly effected by the use of free meshes instead of structured (Appendix A, Table 15 cf. Table 17a), or different 2D stress states (plane strain, antiplane shear, axisymmetric; Appendix A, Tables 17, 18).

<sup>5</sup> In 11 other experiments on 6 problems with power singularities (References 3, 20, 28), (4) indicated not converging in 11/11, then (12) revealed power singularities in 9/11.

### Alternative checks: Divergence detection?

We now use some of our trial problems with power singularities to evaluate the alternative convergence-divergence checks. In this evaluation, we are interested to see if these alternatives reject peak stresses because they are diverging, or at least because error levels are unsatisfactory.

We first apply the linearly increasing mesh sequence of (16) to the same bimaterial corner problem as in Figure 3 and Table 3. This problem has two quite strong singularities (see (47)): Hence diverging stresses should be readily detected by an effective convergence-divergence check. The FEA employs free meshes of 6T elements with  $N_1 = 128$  (see Reference 17 for further specifics). Results for peak stresses are given in Table 6 wherein  $m$  is as in (49).

**Table 6: Divergence detection for a bimaterial corner under tension ( $E_+/E_- = 16$ )**

$m$	$\bar{\sigma}_{\max}$	$\Delta\bar{\sigma}_{\max}$	$\hat{\epsilon}$
1	8.82	1.24	-
2	10.06	0.87	
3	10.93	0.63	0.08
4	11.56		0.05

Clearly in Table 6, the stress increments  $\Delta\hat{\sigma}_{\max}$  are monotonically decreasing with mesh refinement. Thus (4) and (6) are complied with on either the mesh sequence  $N_1, 2N_1, 3N_1$  or  $2N_1, 3N_1, 4N_1$ , and these FEA stresses are predicted to be converging. Then applying (22) gives  $\hat{\epsilon}$  as in Table 6, and a satisfactory ultimate error level on the first sequence, a satisfactory and approaching good level on the second. Hence here this alternative convergence-divergence check would have the stress analyst accept finite stress values as satisfactory when in fact the stress is infinite. Furthermore, the same erroneous conclusions are reached with this check on the same mesh sequence for two other corner problems with strong singularities (see Appendix A, Table 15). As earlier, therefore, an inability of this alternative check to detect divergence and a nonconservative failure as a check. Given this continued failure, we henceforth dispense with any further assessment of this linearly-increasing-mesh-sequence alternative.

We next apply the two-mesh check to the stresses in Table 4. Then the counterpart of (22) realizes the following successive estimates as the mesh number  $m$  increases:

$$\hat{\epsilon} = 0.02, 0.02, 0.02, 0.03 \quad (58)$$

Hence all stresses would be judged converged to within a good level of accuracy. Similarly, applying the two-mesh check to the stresses in Table 5 realizes:

$$\hat{\epsilon} = 0.10, 0.07, 0.06, 0.06 \quad (59)$$

Hence, while the first estimate, being unsatisfactory, would incur further refinement, subsequent stresses would be judged converged to within a satisfactory level of accuracy. As earlier, therefore, an inability of this alternative check to reject divergent stresses and a nonconservative failure as a check. Given this continued failure, we henceforth dispense with any further assessment of this two-mesh alternative.

# Numerical experiments: Diverging stresses with logarithmic singularities

## Contact problems

We start an assessment of the performance of the modified convergence-divergence checks on trial problems with log singularities by examining FEA results for peak contact stresses when an elastic half-space is indented by a smooth rigid wedge (Figure 5). In the FEA of this plane strain problem, the finite region  $R$  for analysis simply has roller supports on its underside, and symmetry conditions on its vertical boundary down the center of the configuration with stress-free conditions on its other vertical boundary. With coordinates as in Figure 5, the maximum, normalized contact stress sought is

$$\bar{\sigma}_{\max} = -\sigma_z (\text{at } x = z = 0) / p \quad (60)$$

wherein  $p$  is the average pressure on the wedge. This stress has a logarithmic singularity akin to that of (1). From Sneddon (Reference 2, Section 48.4),

$$\sigma_s = \text{ord}(E\phi \ln r) \text{ as } r \rightarrow 0 \quad (61)$$

where  $E$  is Young's modulus of the half-space, and now  $\phi$  is the gap angle shown in Figure 5 and  $r$  is a dimensionless radial coordinate as in the same figure.

Analysis uses 4Q host elements in conjunction with surface-to-surface contact elements (CONTA171 and TARGE169, Reference 15), and a contact algorithm with a Lagrange multiplier on the contact normal and penalty on tangent (Reference 15).<sup>6</sup> The rigid wedge is simulated with 4Q elements and a Young's modulus of  $10^6 E$ . The initial mesh for the half-space is uniform with  $N_1 = 400$ , while the mesh for the wedge has but 10 elements with lower nodes aligned with half-space surface nodes. Subsequent meshes for both have element numbers as in (52). Thus meshes in compliance with (3) for  $\lambda = 2$ . Results for  $\bar{\sigma}_{\max}$  when  $p/E = 10^{-3}$  and  $\phi = 1^\circ$  and  $2^\circ$  are given in Table 7 (corresponding gap angles are indicated in parentheses).

---

<sup>6</sup> The default contact algorithm in ANSYS (the augmented Lagrangian algorithm) can produce similar results to those in Table 7, but requires finer meshes to rid the normal contact stress of spurious tensile results.

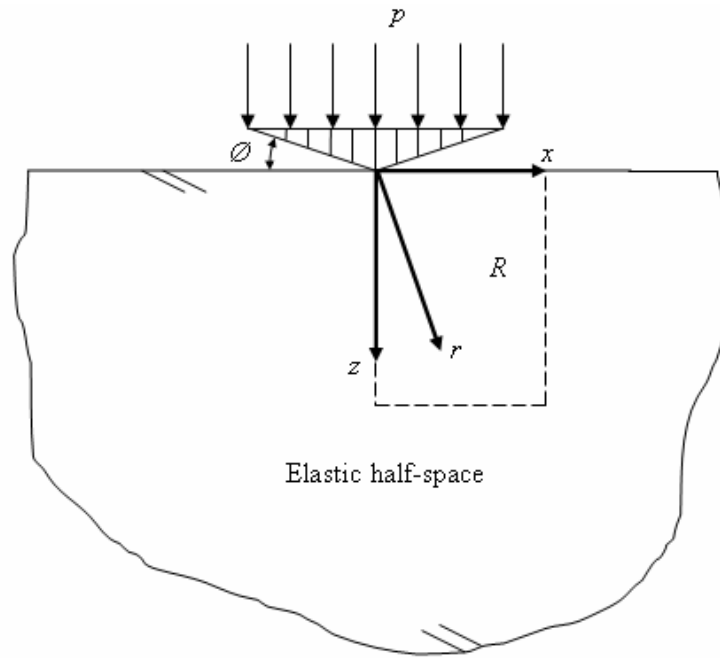


Figure 5. Elastic half-space indented by a smooth rigid wedge

Table 7: Divergence detection for wedge indentation

$m$	$\bar{\sigma}_{\max} (1^\circ)$	$\Delta \bar{\sigma}_{\max}$	$\bar{\sigma}_{\max} (2^\circ)$	$\Delta \bar{\sigma}_{\max}$
1	1.698		1.588	
		2.45		3.77
2	4.145		5.356	
		4.33		8.03
3	8.477		13.39	
		5.16		9.16
4	13.64		22.55	
		5.03		9.08
5	18.67		31.63	

For the  $1^\circ$  stresses in Table 7 on mesh sequences 1,2,3 and 2,3,4, (6) is complied with but (4) is not, so diverging stresses are predicted. Checking (12) and (14) shows that neither are complied with, so nonconvergent stresses are predicted rather than a log singularity. Nonetheless the stresses from either of these two sequences would still be not acceptable. On the mesh sequence 3,4,5, both (4) and (6) are strictly complied with and converging stresses predicted. However, from (20),  $c$  is low (0.04), and consequently from (24),  $\bar{\epsilon} = 9.58$ , a most unsatisfactory level. Further, checking (14) finds it to hold (as has to be the case whenever  $c < 1/7$  for  $\lambda = 2$ ), and a log singularity is thus correctly predicted.

For the 2° stresses in Table 7, like predictions follow: That is, nonconvergent stresses on meshes 1,2,3 and 2,3,4, and a log singularity on meshes 3,4,5. The contact stress for mesh 5 also approaches being double that for a 1° gap, in accordance with (61).<sup>7</sup>

### Other problems

As a first other trial problem with a log singularity, we consider FEA results for the peak principal stress at a step shear on a half-space (Figure 6). In this plane strain problem, the square region  $R$  for analysis has roller restraints on its left-hand vertical boundary and stress-free conditions otherwise except for the application of the shear traction  $\tau_0$ . From Kolosoff (Reference 30), this configuration has a log singularity with

$$\sigma_s = \text{ord}(\tau_0 \ln r) \text{ as } r \rightarrow 0 \quad (62)$$

where  $r$  is a dimensionless radial coordinate as in Figure 6.

The FEA of this configuration uses 4Q elements with  $N_1=16$  and subsequent meshes having element numbers as in (52). Again, therefore, meshes as in (3) for  $\lambda = 2$ . Results are as in Table 8, wherein

$$\bar{\sigma}_{\max} = \sigma_p (\text{at } x = y = 0) / \tau_0 \quad (63)$$

with  $\sigma_p$  being the maximum principal stress, and the coordinates are as in Figure 6.

**Table 8: Divergence detection for step shear**

$m$	$\bar{\sigma}_{\max}$	$\Delta \bar{\sigma}_{\max}$
1	1.122	
		0.226
2	1.348	
		0.240
3	1.588	
		0.229
4	1.817	
		0.350
5	2.167	

<sup>7</sup> With an earlier ANSYS contact element (*circa* 1995), more nearly constant stress increments were found and log singularities predicted in 3 of 3 wedge problems (Reference 29).

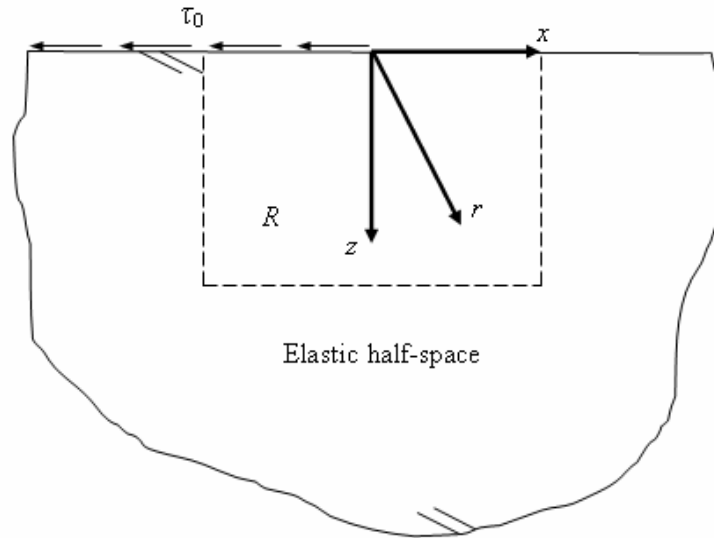


**Figure 6. Elastic half-space under a step shear traction**

On the mesh sequence 1, 2, 3, (6) is complied with but (4) is not, so diverging stresses are predicted. Checking (12) finds it not to be satisfied, so no power singularity is predicted. Checking (14) finds it to be satisfied, so a log singularity is correctly predicted. On the mesh sequence 2, 3, 4, both (4) and (6) are complied with, so converging stresses are erroneously predicted. Estimating the effective convergence rate from (20) gives  $c = 0.07$ , hence, from (24),  $\tilde{\epsilon} = 2.53$ , a most unsatisfactory error level and the stress for mesh 4 should not be accepted. Here, given the low  $c$ , we can also check (14): We find (14) to be satisfied, so that ultimately a log singularity is correctly predicted. On the mesh sequence 3, 4, 5, (6) is complied with but (4) is not, so diverging stresses are predicted. Checking (12) finds it not to be satisfied, so no power singularity is predicted. Checking (14) also finds it to be not satisfied, so no log singularity is predicted. Despite this last incorrect prediction, the stresses on this sequence should still be viewed as nonconvergent and therefore not acceptable.

Similar performance of the modified convergence-divergence checks is found for log singularities induced by the use of displacement shape functions in boundary conditions in submodeling (see Reference 31 for singular fields). Stress results for two normalized stress components at two nodes in two stress concentration ( $K_T$ ) problems are given in Appendix A, Table 19 (from calculations for Reference 31). Log singularities are only detected in 4/12 experiments, although stresses would be judged unacceptable in 11/12 experiments. This does mean, though, that one stress would be judged converging and converged ( $\bar{\sigma}_x$  at  $N_2$  for  $K_T = 5.6$ ), when, in fact, this stress is logarithmically infinite. However, at  $N_2$ ,  $\sigma_y$  would be judged logarithmically singular, so no stress component should be acceptable at this location. Nonetheless, results for  $\bar{\sigma}_x$  at  $N_2$  serve notice of the possibility of nonconservative errors when using these checks on problems with weak log singularities.

## Numerical experiments: Converging stresses

### *Simple problems*

We begin the evaluation of the modified convergence-divergence checks on converging test problems with arguably the simplest class of 2D problems, namely those entailing polynomial stress distributions. For this class, stress fields are continuously differentiable so that FEA convergence should proceed smoothly and

convergence checks work well. In some sense, then, satisfactory performance here is a minimal requirement for these checks.

After Timoshenko and Goodier (Reference 32, Section 18), the polynomial stress fields used here are generated from an Airy stress function  $\chi$  given by

$$\chi = \frac{\sigma_1}{2l} xy^2 + \frac{\sigma_2}{6l^2} (3x^2y^2 - y^4) + \frac{\sigma_3}{20l^3} (y^5 - 5x^4y) \quad (64)$$

wherein  $\sigma_1, \sigma_2$  and  $\sigma_3$  are constants representative of applied tractions for stress fields with first-order, second-order and third-order polynomials. These fields act within the elastic plate  $R$  of Figure 2. To pose associated test problems, corresponding tractions are applied on  $x = 2l, y = l$ , and appropriate symmetry/antisymmetry conditions on the  $x, y$  axes. We thus have true test problems with the polynomial stress fields constituting the exact solutions throughout the elastic plate. Uniform meshes of 4Q and 8Q elements with initial mesh refinement as in Figure 2 are used in the FEA of these test problems. A total of 26 such meshes are run on the three polynomial problems. Viewing one three-mesh sequence for a single stress component as a single experiment, these meshes give rise to 38 experiments. Here we present sample results, then merely summarize the performance of the modified convergence-divergence checks re convergence assessment (companion detailed results are set out in Appendix B, Table 20).

The selected polynomial problem is the third-order problem because it presents the greatest challenge to FEA. This problem has antisymmetry conditions on the  $x$  axis, symmetry conditions on the  $y$  axis, and prescribed tractions from (64) with  $\sigma_1 = \sigma_2 = 0$  on the other boundaries. The key local stresses sought are:

$$\begin{aligned} \bar{\sigma}_x &= \sigma_x(\text{at } x = 0, y = l) / \sigma_3 = 1 \\ \bar{\tau}_{xy} &= \tau_{xy}(\text{at } x = 2l, y = 0) / \sigma_3 = 8 \end{aligned} \quad (65)$$

The FEA reported here uses 4Q elements with  $N_1 = 8$  and subsequent element numbers as in (52). Thus meshes as in (3) with  $\lambda = 2$ . Results for  $\bar{\sigma}_x$  and  $\bar{\tau}_{xy}$  are included in Table 9.

**Table 9: Convergence assessment for third-order polynomial problem**

$m$	$\bar{\sigma}_x$	$\Delta \bar{\sigma}_x$	$\bar{\tau}_{xy}$	$\Delta \bar{\tau}_{xy}$
1	2.3849		5.3000	
		1.0084		1.2929
2	1.3765		6.5929	
		0.2796		0.6838
3	1.0969		7.2767	
		0.0725		0.3555
4	1.0244		7.6322	
		0.0183		0.1822
5	1.0061		7.8144	
		0.0046		0.0923
6	1.0015		7.9067	

For  $\bar{\sigma}_x$ , the stress increments in Table 9 have (4) and (6) being complied with and converging stresses correctly predicted on all four three-mesh sequences. Then using (20) gives  $c \approx 2$  so that, for 4Q elements, (22) applies. For the three-mesh sequences starting with meshes 1, 2, 3, and 4, in turn, this gives

$$\hat{e} = 0.25, 0.07, 0.02, 0.005 \quad (66)$$

In fact, actual absolute relative errors are

$$|\bar{e}| = 0.10, 0.02, 0.006, 0.002 \quad (67)$$

Hence error estimates that are uniformly conservative, as could be expected with  $c \approx 2$  and 4Q elements. Error levels are also conservative but are comparable: for meshes 1, 2, 3, unsatisfactory error is predicted whereas the actual error is barely satisfactory; for 2, 3, 4, satisfactory is predicted whereas actual is good; for 3, 4, 5, good is predicted whereas actual is excellent; and for 4, 5, 6, excellent is predicted as is actually the case (recall the classification of error levels following (5)).

For  $\bar{\tau}_{xy}$ , the stress increments in Table 9 have (4) and (6) being complied with and converging stresses correctly predicted on all four three-mesh sequences. Now using (20) gives  $c$  just less than 1 so that (24) applies. For the mesh sequences in turn this gives

$$\bar{e} = 0.11, 0.05, 0.02, 0.01 \quad (68)$$

In actuality,

$$\bar{e} = 0.09, 0.05, 0.02, 0.01 \quad (69)$$

Hence still conservative but now closer with predicted error levels being the same except for meshes 1, 2, 3, whereon unsatisfactory error is predicted whereas actual error is barely satisfactory.

For other polynomial problems and stresses (see Appendix B, Table 20), (4) and (6) are complied with in 28/30 experiments, and converging results correctly predicted. For the other two experiments ( $m = 1-4$  for  $\sigma_{x_2}$  in Table 20a), sign changes in stress increments on the first three meshes have (6) not being complied with so our converging check (4) is not applicable. Thereafter on the next three meshes when (6) is complied with, (4) is not, and nonconvergence predicted (neither a power nor a log singularity is predicted). Ultimately, on the next three meshes, convergence is correctly predicted. In fact, this stress on the initial mesh sequence is diverging as a result of oscillatory errors. Hence the convergence-divergence checks are not seriously awry in making a prediction of temporary nonconvergence that is late by one mesh.

For these other polynomial problems when convergence is predicted, error estimates are uniformly greater than or equal to actual errors. Moreover, these estimates are typically more accurate than those of (66), with predicted error levels being the same as actual for all 28 experiments. All told, a conservative and quite satisfactory performance of the modified convergence-divergence checks on these elementary polynomial problems.

Another simple class of problems for 2D stresses can be obtained by drawing on the theory of thick-wall pressure vessels. What makes these problems simple is that the stresses, in addition to being continuously differentiable throughout a vessel, depend on just a single coordinate. In some sense, therefore, these could be viewed as 1D problems.

For an elastic pipe under constant internal pressure  $p$  (Figure 7), exact solutions for the radial and hoop stresses may be found in Timoshenko and Goodier (Reference 32, Section 28). For a specific pair of radii ratios ( $r_o/r_i$ ), an FEA is described in Reference 33. Results of this FEA for what are, in effect, four numerical experiments are given in Appendix B, Table 21. For all four experiments, (4) and (6) are complied with and converging FEA stresses correctly predicted. Too, in all four experiments for this elementary class of problems, error estimates are correctly predicted to attain excellent levels.

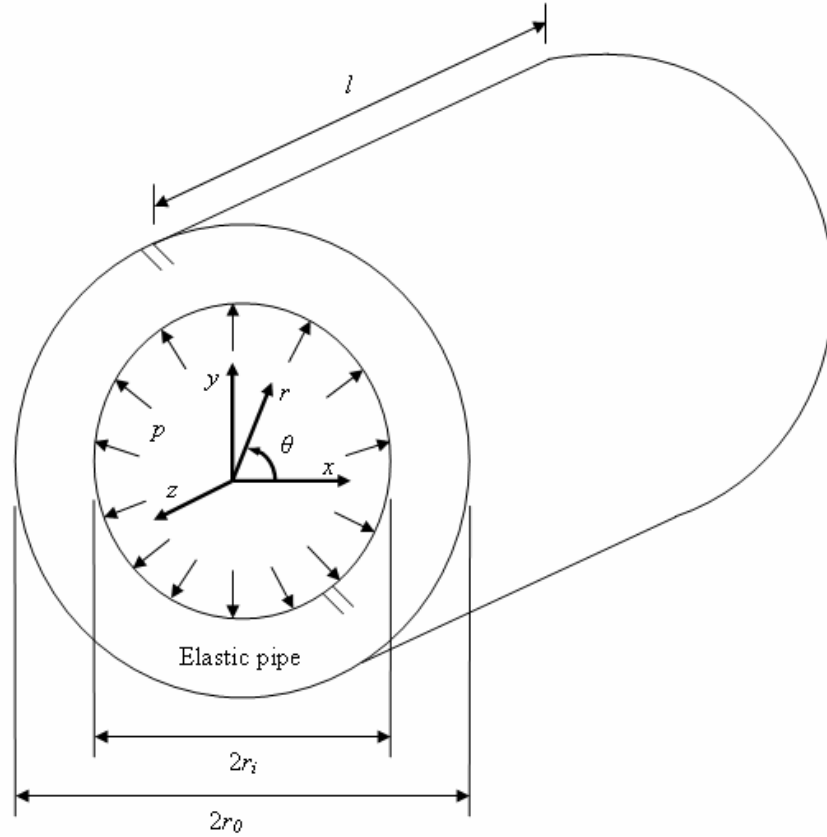


**Figure 7. Elastic pipe under internal pressure**

A more challenging pressure vessel problem with varying internal pressure can be constructed using Love's stress function (see, e.g., Reference 32, Section 131). Letting  $\chi$  now denote this axisymmetric biharmonic function, a separable solution is

$$\chi = C_3 p_r l^3 [2\nu \cos \zeta + \zeta \sin \zeta] [I_0(\rho)K_1(1) + I_1(1)K_0(\rho)] \quad (70)$$

where  $C_3 = 3.46122 \times 10^{-2}$ ,  $p_r$  is a representative pressure,  $\zeta = \pi z/l$ ,  $\rho = \pi r/l$ , with  $z, r$  being as in Figure 7, and  $I, K$  are modified Bessel's functions of the first, second kinds. Obtaining stresses from  $\chi$  using standard formulae and applying appropriate components as tractions on the boundaries in Figure 7, then provides a test problem (see Reference 33 for details). These same stresses constitute the exact solution for this test problem. Specifically we take  $r_i/l = \pi^{-1}$  and  $r_o/l = \pi^{-1} + 1/2$  to simplify the expressions involved, and set  $\nu = 0.3$ . Then we discretize the rectangular area constituting a cross section of the pipe between  $x = r_i$  and  $x = r_o$  and between  $z = 0$  and  $z = l$  (Figure 7) with uniform meshes of 4Q elements. The FEA that follows uses  $N_1 = 8$  and subsequent  $N$  as in (52), thus refinement as in (3) with  $\lambda = 2$  (see *ibid* for details). Results for the normalized hoop stress  $\bar{\sigma}_\theta$  are included in Table 10, with  $\bar{\sigma}_\theta$  being defined as

$$\bar{\sigma}_\theta = \sigma_\theta(\text{at } r = r_o, z = l) / p_r = 2.0681 \quad (71)$$

**Table 10: Convergence assessment for pipe under varying pressure**

$m$	$\bar{\sigma}_\theta$	$\Delta\bar{\sigma}_\theta$	$c$	$\hat{\epsilon}$	$ \bar{\epsilon} $
1	3.0571				
		-0.8933			
2	2.1638		2.18		
		-0.1977		0.10	0.05
3	1.9661		na		
		0.0035			
4	1.9696		nc		
		0.0268			
5	1.9964		2.11		
		0.0062		0.003	0.03
6	2.0026				

In actuality for  $\bar{\sigma}_\theta$  of Table 10, FEA results are converging on the first two meshes, diverging on the next two, and converging thereafter. This somewhat erratic convergence pattern is a consequence of the oscillatory nature of the errors here. As earlier with one polynomial problem, it causes some difficulty for our convergence-divergence checks. Initially they predict convergence ( $c \approx 2$ ), then they are not applicable (na) because of sign changes in stress increments, then they predict nonconverging (nc) but not diverging due to a singularity, and finally, correctly, converging. When converging is predicted, error estimates are as in Table 10 and are initially conservative but ultimately nonconservative. However, the ultimate estimate only underestimates error by one level, predicting excellent when in fact the error is but good. Again, therefore, a demonstration of some wayward predictions but eventually satisfactory performance of the convergence-divergence checks in the presence of oscillatory errors.

### **Stress concentration problems**

In practice, a significant fraction of FEA of 2D elastic stresses is concerned with the determination of stress concentration factors,  $K_T$ . To span the spectrum of  $K_T$  typically met, we next consider an elastic plate with an elliptical hole under a uniform, transverse, far-field tension of magnitude  $\sigma_0$  (Figure 8). An exact solution for this configuration in terms of complex potentials is given in Kolosoff (Reference 30). This solution gives the normalized maximum stress at the ends of the elliptical hole as

$$\bar{\sigma}_{\max} = \sigma_y(\text{at } x = a, y = 0) / \sigma_0 = 1 + 2a/b \quad (72)$$

In (72), coordinates are as in Figure 8. Hence by varying the aspect ratio ( $a/b$ ) of the hole,  $K_T = \bar{\sigma}_{\max}$  can be made to vary. Here we choose four aspect ratios such that  $K_T$  varies from 5 to about 300, a range that encompasses and probably exceeds that usually encountered in practice.

The solution in Kolosoff (Reference 30) is for an infinite elastic plate. To begin to pose problems on finite regions so that we can apply FEA, we take advantage of the symmetry about the  $x$  and  $y$  axes (Figure 8) to restrict attention to a quadrant ( $x > 0, y > 0$ ). Thereafter, however, we need appropriate field variables on a boundary such as the outer elliptical boundary of  $R$  in Figure 8 in order to prescribe boundary conditions there. Such fields are not explicitly given in Kolosoff (Reference 30): They are, though, obtained in Cormier *et al.* (Reference 14). We use the displacements given in Reference 14 to prescribe conditions on this outer boundary and so complete formulations.

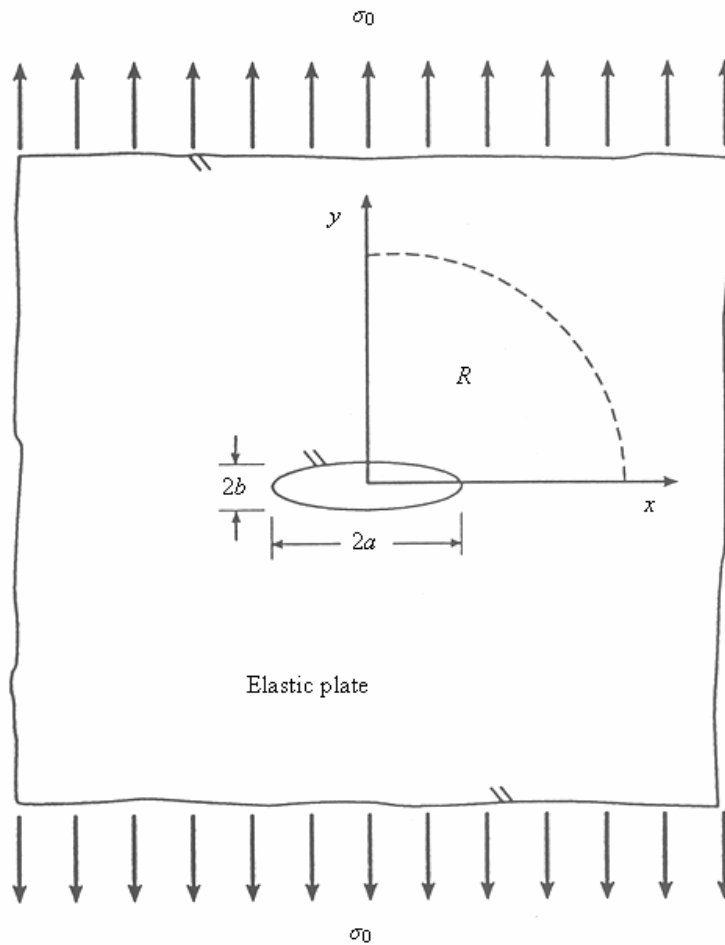


**Figure 8. Elastic plate with an elliptical hole under tension**

For our four elliptical hole problems, we employ a variety of FEA approaches. Here, we give results for structured meshes in elliptical cylindrical coordinates with 4Q and 8Q elements, and for free meshes of 4Q elements with and without adaptive mesh refinement, a total of 65 meshes that together realize 36 numerical experiments. In Reference 11, results are given for submodeling with 4Q and 8Q elements. In what follows, we first present selected results for a structured mesh, then merely summarize the performance of the convergence-divergence checks re convergence assessment for the other FEA (companion detailed results are set out in Appendix B, Tables 22, 23, and Reference 11).

We select results for  $a/b = 52.155$  because this choice leads to a high  $K_T$  or  $\bar{\sigma}_{\max}$ , and so challenges FEA. The chosen FEA uses 4Q elements with nodes specified by elliptical cylindrical coordinates and  $N_1 = 1024$  (see Reference 11 for details). Results for  $\bar{\sigma}_{\max}$  are given in Table 11.

**Table 11: Convergence assessment for plate with elliptical hole ( $K_T = 105.31$ )**

$m$	$\bar{\sigma}_{\max}$	$\Delta\bar{\sigma}_{\max}$	$c$	$\bar{e}, \hat{e}$	$\bar{e}$
1	43.31	22.27			
2	65.58	20.35	0.13		
3	85.93	12.23	0.73	2.51	0.18
4	98.16	4.97	1.30	0.19	0.07
5	103.13	1.58	1.65	0.05	0.02
6	104.71			0.02	0.01

For all four three-mesh sequences available from Table 11, (4) and (6) are complied with and converging stresses correctly predicted. Initial effective convergence rates are estimated to be low, leading to conservative error estimates. However, error levels are comparable, both estimated and actual error being unsatisfactory for the first sequence, and estimated error being still unsatisfactory on the second sequence when the error in reality is satisfactory. Later sequences have estimated and actual errors being good, then estimated error being still good while actual error is excellent.

For this problem and other elliptical hole problems analyzed with structured meshes comprised of 4Q and 8Q elements, (4) and (6) are complied with and correctly predict converging peak stresses in 18/22 experiments (see Appendix A, Table 22 for detailed results). The other four experiments involve a high stress concentration ( $K_T = 296$ ) and entail meshes which are relatively coarse compared to those ultimately required for the accurate determination of the peak stress. For two of these four cases nonconvergent results are predicted, while for the other two log singularities are predicted, despite stresses actually converging. Notwithstanding these last errant predictions, results for all four have quite unsatisfactory actual error levels and so should not be accepted anyway.

For the 18 experiments in which (4) and (6) are complied with, error levels predicted by (22), (24) or (25) are the same as actual levels in 14 experiments, one level higher in 3 experiments, and two levels higher in 1 experiment. These last overestimates could occasion some additional computation that is unnecessary. Even so, we view the performance of the modified convergence-divergence checks on the elliptical hole problems when analyzed with structured meshes as satisfactory. This is because they would not see a stress analyst accept unacceptable stress results as acceptable, and they do provide conservative yet fairly accurate error estimates when stresses are judged converging.

Using the AMESH command (Reference 15), free meshes are typically relatively easy to implement compared to structured meshes. On the other hand, they do not enjoy the mesh refinement near the peak stress location effectively produced by the use of structured meshes with nodes placed at uniform increments of elliptical cylindrical coordinates (see Reference 11, Figure 3). Consequently, we just consider free meshes for the two elliptical hole problems with the lower peak stresses ( $K_T = 5.61, 37.88$ ; see Appendix A, Tables 22a, b for results with 4Q elements). For these two problems, (4) and (6) correctly predict convergence in but 2 of 4 experiments. For these two experiments, error levels predicted by (22) and (24) are the same as actual levels. For the other two experiments, the free meshes used are effectively too coarse to capture the peak stress involved ( $K_T = 37.88$ ). Accordingly, while a power singularity and nonconvergent results are predicted instead of converging results, actual error levels are too high for

stresses to be accepted anyway. Overall, a satisfactory performance by the modified convergence-divergence checks.

Given the high  $K_T$  involved in most of the elliptical hole problems, it makes sense to consider the use of free meshes in conjunction with adaptive mesh refinement. To this end we employ the macro ADAPT (Reference 15), which is based on Zienkiewicz and Zu (References 9, 10), to improve analysis with free meshes for  $K_T = 37.88, 105.31$  and  $296.04$ . Further specifics of this FEA with 4Q elements are given in Reference 11 (see Appendix A, Table 23 for detailed results so calculated). For these three problems, (4) and (6) correctly predict convergence in 6/6 experiments. Then if (25) is used in addition to (22) and (24) to take advantage of increased convergence rates with adaptive mesh refinement, error levels are predicted to be the same as actual in 2/6 experiments, one level higher in the other 4 experiments. Overall, a satisfactory performance by the modified convergence-divergence checks.

An alternative means of improving resolution of the peak stresses in the ellipse problems is via submodeling or rezoning. This is performed with 4Q and 8Q elements in Reference 11. Results there have (4) and (6) complied with and therefore correctly predicting convergence in 8/8 experiments. Then applying (20), (24) and (25) gives predicted error levels that are the same as actual in 6/8, and one level higher for the other 2. Overall, again satisfactory performance.

### **Contact problems**

In practice, contact problems are also a common application of FEA. This class of problem can present two challenges to FEA: numerical determination of contact extents, and numerical resolution of stress concentrations.<sup>8</sup> The first can lead to oscillatory convergence and consequent difficulties in assessing errors (*cf.*, Table 10). The second can require extensive mesh refinement for convergence (*cf.*, Table 11).

A generic conforming-contact configuration that can include both challenges is the elastic half-space indented by a smooth rigid punch with a flat base and rounded edges (Figure 9). Herein, an FEA has to determine the extent of contact outside of the flat width  $2w$ . If an FEA underestimates this extent, it can begin to converge on too high a contact stress, and, conversely, if it overestimates, too low. As contact extents are successively numerically approximated then, convergence of peak contact stresses need not be monotonic. Herein, too, as the edge radius,  $r_e$ , is reduced, high contact stresses occur near the edges of contact. Indeed for  $r_e = 0$ , these stresses are singular (*cf.*, Appendix A, Table 18).

Exact solutions for the conforming-contact configuration of Figure 9 are available. For  $w = 0$ , we have solutions for indentation by a sphere (axisymmetric case) or a cylinder (plane strain case) from Hertz (as reported in Reference 34, Appendix 3). For  $w \neq 0$ , we have solutions for indentation by a strip punch (plane strain case) from Steuermann (as reported in Reference 35). Thus such configurations can potentially serve as test problems.

---

<sup>8</sup> For contact with friction, there is the further challenge of numerically policing friction laws: We do not consider this additional challenge here.

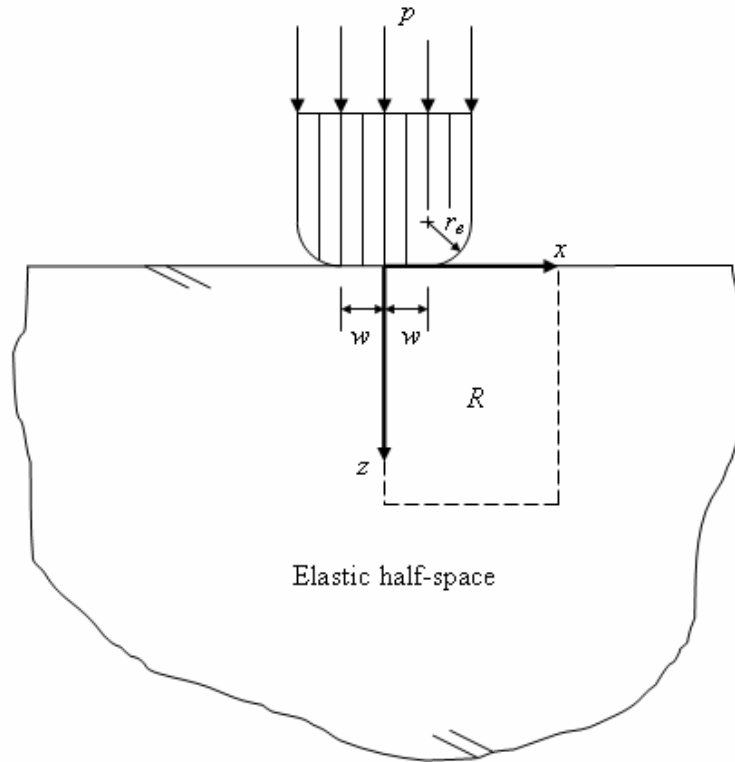


**Figure 9. Elastic half-space indented by a smooth rigid punch with rounded edges**

For FEA, we select both axisymmetric and plane strain cases for  $w/r_e = 0$ , then five other values of  $w/r_e \neq 0$ , one with two different indentation pressures  $p$  and hence two different  $K_T$ . This selection gives rise to a total of eight contact problems with  $K_T$  varying from 1.3 to about 30, a range likely to include most contact stress concentrations encountered in practice.

To pose contact problems on finite regions such as  $R$  of Figure 9, we first exploit symmetry to provide conditions on the  $z$  axis. Next, we could attempt to draw on internal stresses in the half-space to provide counterbalancing tractions on the remainder of the interior boundary of  $R$ . For Hertzian contact of a cylinder, simple expressions for such stresses are available from McEwen (as reported in Reference 34, Section 4.2), and we use them to provide tractions. For the other contact problems, no such simple expressions would appear to be available. For these problems, therefore, we employ conditions on the other interior boundaries of  $R$  that are asymptotically correct in a St. Venant sense. We do this by drawing on stresses from known exact solutions for surface forces/tractions acting on an elastic half-space. We use these stresses to apply tractions on the interior of  $R$  that counterbalance the force exerted by the indenter. We start with  $R$  of extent say  $l$  deep and wide, then successively double  $l$  until negligible differences occur in the FEA of the sought-after contact stress.

For our eight contact problems, we use predominantly 4Q host elements in conjunction with surface-to-surface contact elements. Given  $c \approx 1/2$  at the edges of contact, we do not expect 8Q elements to offer any significant improvement in convergence, though we check this expectation out on one contact problem. We use the default contact algorithm (the augmented Lagrangian algorithm, Reference 15) for the Hertzian contact problems, the contact algorithm with a Lagrangian multiplier on the contact normal and penalty on tangent (Reference 15) for the Steuermann contact problems because it performs better on these problems (see Reference 20). The rigid punches are simulated with a Young's modulus of  $10^6 E$  and the same host elements as the half-space. Initial meshes are uniform for Hertzian contact but have some local refinement near the edge of contact for Steuermann contact. Subsequent meshes all have host element numbers as in (52): thus mesh refinement as in (3) with  $\lambda = 2$ . A total of 29 meshes are run that together realize 13

numerical experiments. In what follows, we first present results for one Hertzian and two Steuermann problems, then merely summarize the performance of the modified convergence-divergence checks re convergence assessment for the other FEA (companion detailed results are set out in Appendix B, Tables 24, 25).

For the one axisymmetric Hertzian problem, results for the peak, normalized, contact stress  $\sigma_c$  are included in Table 12, with  $\bar{\sigma}_c$  being defined as

$$\bar{\sigma}_c = -\sigma_z \text{ (at } x = r = 0, z = 0) / p = 1\frac{1}{2} \quad (73)$$

where  $x, z$  are as in Figure 9, the radial coordinate  $r$  for the axisymmetric problem is taken to coincide with  $x$ , and the exact value is from Reference 34, Appendix 3. The far-field boundary conditions employ the Boussinesq solution for a point-load on a half-space (see, e.g., Reference 34, Section 3.2) with extents of  $R$  being eight times the contact radius. The FEA starts with a uniform mesh of 4Q elements for the half-space with  $N_1 = 256$  (see Reference 20 for details).

**Table 12: Convergence assessment for Hertzian spherical contact**

$m$	$\bar{\sigma}_c$	$\Delta\bar{\sigma}_c$	$c$	$\hat{e}$	$\bar{e}$
1	1.1992				
		0.1938			
2	1.3930		1.20		
		0.0841			
3	1.4771			0.06	0.02

For the three-mesh sequence in Table 12, the stress increments have (4) and (6) being complied with and converging stresses correctly predicted. Thereafter using (22) because  $c > 1$ , error is predicted to be satisfactory when actual error level is good, a conservative result.

Similar performance of the modified convergence-divergence checks occurs for  $\bar{\sigma}_c$  in the other Hertzian contact problem (plane strain cylinder). For the two three-mesh sequences for  $\bar{\sigma}_c$  available from Appendix B, Table 24, (4) and (6) are complied with and correctly predict converging stresses (despite one instance of oscillatory actual errors). Error levels predicted for  $\bar{\sigma}_c$  agree with actual, both being excellent (actual errors being slightly higher for 8Q elements than 4Q). All told, a conservative and quite satisfactory performance of the modified convergence-divergence checks for  $\bar{\sigma}_c$  in Hertzian contact.

On the other hand, performance for the peak, horizontal, contact stress in the cylindrical Hertzian problem is not so good. While convergence is correctly predicted by (4) and (6) for the two three-mesh sequences in Table 24, errors from (22) and (24) are underestimates. Errors are predicted to attain excellent levels when in fact they are but good (actual errors being very slightly higher for 8Q elements than 4Q). This represents a nonconservative failure of the modified convergence-divergence checks, albeit not a gross failure. It is caused by  $c$  of (20) significantly overestimating actual convergence rates (recall discussion following (25)). Here, as elsewhere, FEA can have difficulty determining this contact stress component, and actual convergence rates can be low ( $\approx 0.1$ ).

For two Steuermann problems, results for the peak, normalized, contact stress  $\bar{\sigma}_c$  are included in Table 13, with  $\bar{\sigma}_c$  now being defined as

$$\bar{\sigma}_c = -\bar{\sigma}_z \text{ (max imum value on } x > 0, z = 0) / p \quad (74)$$

where coordinates are as in Figure 9. The far-field boundary conditions employ the Michell solution for a uniform pressure over a strip on a half-space (see, e.g., Reference 34, Section 2.5). One of these problems has gently rounded edges ( $w/r_e = 7/9$ ), the other sharply rounded ( $w/r_e = 97/3$ ). Corresponding exact solutions for  $\bar{\sigma}_c$  of (74) are developed by Steuermann and may be obtained from Reference 35. These solutions locate  $\bar{\sigma}_c$  of (74) near the edge of contact for both problems. They depend not only on the degree of roundness but also on load level and Poisson's ratio. For the results in Table 13,  $\nu = 0.42$ . Then corresponding exact values of  $\bar{\sigma}_c$  for respective edge roundness and load levels are:

$$\begin{aligned} w/r_e = 7/9, p/E = 1/1243, \bar{\sigma}_c = 6.7032 \\ w/r_e = 97/3, p/E = 1/2718, \bar{\sigma}_c = 29.908 \end{aligned} \quad (75)$$

The FEA for these peak  $\bar{\sigma}_c$  starts with a nonuniform mesh of 4Q elements with  $N_1 = 2000$  for both problems (see Reference 20, Figure 3(c), for an example of the local mesh refinement used near the edge of contact). Results so produced are included in Table 13 distinguished by  $w/r_e$  ratios in parentheses.

For the two three-mesh sequences for  $w/r_e = 7/9$  in Table 13, the stress increments have (4) and (6) being complied with and converging stresses correctly predicted. Then (22) furnishes the successive error estimates

$$\hat{e} = 0.02, 0.005 \quad (76)$$

In fact

$$\bar{e} = 0.008, 0.003 \quad (77)$$

Hence initially a conservative prediction of a good error level when in fact the error level is excellent, and ultimately a prediction of excellent when so. For this problem, then, a satisfactory performance of the modified convergence-divergence checks.

For the first three-mesh sequence for  $w/r_e = 97/3$ , (6) is complied with but (4) is not so that divergence is predicted. Neither (12) nor (14) is met, so nonconvergent results are predicted rather than divergence due to a stress singularity. For the second three-mesh sequence, (6) is not complied with and the modified convergence-divergence checks are not applicable. In fact, stresses are converging on meshes 1, 2, diverging on meshes 2, 3 because of oscillatory errors, and ultimately converging on meshes 3, 4 to within

**Table 13: Convergence assessment for Steuermann contact**

$m$	$\bar{\sigma}_c(7/9)$	$\Delta\bar{\sigma}_c$	$\bar{\sigma}_c(97/3)$	$\Delta\sigma_c$
1	6.3435		27.617	
		0.1714		1.320
2	6.5149		28.937	
		0.1314		1.980
3	6.6463		30.917	
		0.0364		-1.029
4	6.6827		29.888	

an error of 0.07%. This is an example of the nonmonotonic convergence that can occur in contact problems (in our experience, about one time in four). As earlier, this causes difficulties for the modified convergence-divergence checks (*cf.*, Table 10) and they fail to discern that stresses here have actually converged to within an excellent error level.

Similar performance of the modified convergence-divergence checks to that for  $\bar{\sigma}_c$  (7/9) of Table 13 occurs for  $\bar{\sigma}_c$  in the other Steuermann problems. For the four three-mesh sequences for  $\bar{\sigma}_c$  available from Appendix B, Table 25, (4) and (6) are complied with and correctly predict converging stresses (actual convergence is monotonic in this table). Error levels predicted agree with actual, all being good. Overall, then, a conservative and quite satisfactory performance of the modified convergence-divergence checks for  $\bar{\sigma}_c$  in Steuermann contact when convergence is monotonic.

## Concluding remarks

Determining whether key elastic stresses computed via FEA are diverging or converging is essential for their meaningful use in engineering practice. If converging, the further determination of the degree to which they have converged is a prerequisite to their successful use. To these ends and in light of the results found in this paper, we recommend the adoption of the *convergence-divergence checks* summarized in what follows.

For these checks, at the outset the FEA should be carried out on at least *three* meshes that are formed by successive, systematic, *scaled* refinement. That is, if  $h$  is a linear measure of representative element size in the first coarse mesh, subsequent medium and fine meshes should have element sizes  $h/\lambda$  and  $h/\lambda^2$ , where  $\lambda$  is the scale factor. As a minimum,  $\lambda$  should be no less than 3/2; typically  $\lambda \approx 2$ . On these three meshes, an FEA calculation of the key stress  $\sigma$  is made (at a common location), yielding  $\sigma_c$ ,  $\sigma_m$  and  $\sigma_f$ , respectively. Thereafter, increments in  $\sigma$  are determined in accordance with

$$\Delta\sigma_c = \sigma_m - \sigma_c, \Delta\sigma_m = \sigma_f - \sigma_m \quad (78)$$

These two increments must not be of opposite signs for the checks to be applicable: If they are, further refinement is required until they are not.

Given  $\Delta\sigma_c \Delta\sigma_m \geq 0$ , three cases can be distinguished:

$$(i) \quad |\Delta\sigma_c| < |\Delta\sigma_m| \dots \text{diverging} \quad (79)$$

$$(ii) \quad |\Delta\sigma_c| \approx |\Delta\sigma_m| \dots \text{diverging} \quad (80)$$

$$(iii) \quad |\Delta\sigma_c| > |\Delta\sigma_m| \dots \text{converging} \quad (81)$$

We expand on these three cases in turn.

For Case (i), stresses may be diverging because of the presence of a *power singularity* with  $\sigma = O(r^{-\gamma})$  as  $r \rightarrow 0$ . To check for this possibility, successive estimates of the singularity exponent  $\gamma$  can be made via

$$\hat{\gamma} = [\ln(\sigma_m/\sigma_c)]/\ln \lambda, \tilde{\gamma} = [\ln(\sigma_f/\sigma_m)]/\ln \lambda \quad (82)$$

Then a power singularity is judged to be present when the magnitude of the difference between these two exponent estimates is less than 10% of their mean value. If so, stress values are physically meaningless and their further FEA is useless. If not, stresses may have a log singularity (see next case), or simply not yet be converging/have converged because meshes are too coarse. In this last instance, further FEA can yield physically reasonable results.

For Case (ii), the approximate equality holds whenever the magnitude of any change between  $|\Delta\sigma_c|$  and  $|\Delta\sigma_m|$  is less than 10% of their mean value. Thus Case (ii) includes instances in strict compliance with (79) or (81). When Case (ii) holds, a *log singularity* is judged to be present. That is, stress values which are physically meaningless with  $\sigma = O(\ln r)$  as  $r \rightarrow 0$ .

For Case (iii), given Case (ii) does not hold, stresses are judged to be *converging*. Then an assessment needs to be made of the degree to which stresses have converged.

To assess the degree that stresses have *converged*, first an estimate of the effective convergence rate  $c$  is made via

$$c = [\ln(\Delta\sigma_c/\Delta\sigma_m)]/\ln\lambda \quad (c > 0) \quad (83)$$

Then if  $\lambda^c \geq 2$ , the relative absolute error in  $\sigma_f$  is estimated by

$$\hat{e} = |\Delta\sigma_m/\sigma_f| \quad (\sigma_f \neq 0) \quad (84)$$

If not and  $\lambda^c < 2$ , the error in  $\sigma_f$  is estimated by

$$\bar{e} = \hat{e}/(\lambda^c - 1) \quad (85)$$

Here, when the larger of  $\hat{e}$  and  $\bar{e}$  is less than 0.1, the FEA is judged to have converged to a satisfactory level, when less than 0.05 to a good level, and when less than 0.01 to an excellent level. Certainly, though, other numerical values for these levels could be set.<sup>9</sup> The foregoing summarizes the essential elements of the recommended convergence-divergence checks for divergence detection and convergence assessment. The main body of the paper does contain some improvements (see discussion surrounding (15) and following (25)).

The analogues of these convergence-divergence checks are applied to three series that diverge, three that converge, and one that can do either. They correctly predict divergence for the three divergent series, convergence for the three convergent series, and are conservative as to when convergence occurs for the last series. Thereafter for the three convergent series, they accurately estimate errors for two and overestimate the error for the third.

For 26 numerical experiments on 14 trial problems with power singularities, (79) and (80) detect divergence for 96%. Then using (82), power singularities are predicted for 92% of this 96%. The one experiment erroneously judged to have converging stresses involves a weak singularity ( $\gamma = 0.091$ ).

Ultimately, though, these stresses are not judged converged via (83)-(85), and so would not be accepted, as should be the case.

For 21 numerical experiments on 5 trial problems with log singularities, (79) and (80) detect divergence for 90%. Then using just (80), log singularities are predicted for but 37% of this 90%. This low success rate of predicting actual log singularities may be attributed to the weak nature of these singularities that makes them easily masked. The two experiments erroneously judged to have converging stresses are ultimately judged by the convergence-divergence checks to lead to unacceptable stresses, as should be the case.<sup>10</sup>

For 103 numerical experiments on 18 test problems with nonsingular stresses, (81), with (80) not holding, predicts convergence for 88%. For these experiments wherein stresses are judged converging, (83), (84) and (85) estimate errors to be two levels above actual in 2%, one level above in 18%, the same in 77%, and one level below in 3%. For the other 12 experiments, about half cannot be assessed because of oscillatory errors, while the other half are for stresses on coarse meshes that have yet to converge anyway.

In sum, the foregoing experiments demonstrate that the recommended convergence-divergence checks can perform satisfactorily in 2D stress analysis with finite elements, and so would seem likely to be satisfactory in practice for such analysis. Further study is needed to see if this is so in 3D stress analysis.

---

<sup>9</sup> If instead 0.05, 0.01 and 0.001 are used for satisfactory, good and excellent, performance of the convergence-divergence checks on the trial and test problems is essentially unchanged.

<sup>10</sup> For all singular problems, it is helpful to have asymptotic identifications of singular stresses to confirm FEA suspicions of divergence, and thereby avoid further futile analysis: This is particularly so for log singularities wherein divergence can be hard to detect numerically. Reference 4 provides a recent review of such asymptotics.

The same cannot be said of the alternative checks considered here: the linearly-increasing-mesh-sequence check and the two-mesh check. These are demonstrated here to be unreliable when it comes to detecting divergence and singular stresses, and so not good practice.

## Acknowledgments

We are most grateful to colleagues who assisted with the FEA of trial and test problems: A.J. Birnbaum of Carnegie Mellon University (CMU), butt joint problems; B.P. Epps of CMU, problems with boundary conditions from shape functions; H.R. Gadre of Louisiana State University (LSU), corner problems in antiplane shear; J. Jiang of LSU, Steuermann contact problems; Y. Karpenko of CMU, step shear problem; E.R. Lewis of LSU, pressure vessel problems; Y. Lu of LSU, bimaterial corner problems; and C.W. Rummel of CMU, corner problems in plane strain. We are also grateful to ANSYS Inc., for providing access without charge to their code for the polynomial and elliptical hole problems.

## References

- 1) J.J. Juenger, S.C. Peterson, F.C. Herzner, Stress-relieved rotor blade attachment slot. U.S. Patent Number 5,141,401 (1992).
- 2) I.N. Sneddon, *Fourier Transforms*. McGraw-Hill Book Co., 1951, New York, NY.
- 3) G.B. Sinclair, Stress singularities in classical elasticity – I: Removal, interpretation, and analysis. *Applied Mechanics Reviews*, 2004, Vol. 57, pp. 251-297.
- 4) G.B. Sinclair, Stress singularities in classical elasticity – II: Asymptotic identification. *Applied Mechanics Reviews*, 2004, Vol. 57, pp. 385-439.
- 5) J.E. Akin, *Finite Element Analysis with Error Estimators*. Elsevier Butterworth-Heinemann, 2005, Oxford, England.
- 6) R.D. Cook, D.S. Malkus, M.E. Plesha, R.J. Witt, *Concepts and Applications of Finite Element Analysis* (4<sup>th</sup> edition). John Wiley & Sons, Inc., 2002, New York, NY.
- 7) J.N. Reddy, *An Introduction to the Finite Element Method* (3<sup>rd</sup> edition). McGraw-Hill Companies, 2006, New York, NY.
- 8) O.C. Zienkiewicz, R.L. Taylor, J.Z. Zhu, *The Finite Element Method: Its Basis and Fundamentals* (6<sup>th</sup> edition). Elsevier Butterworth-Heinemann, 2005, Oxford, England.
- 9) O.C. Zienkiewicz, J.Z. Zhu, A simple error estimator and adaptive procedure for practical engineering analysis. *International Journal for Numerical Methods in Engineering*, 1987, Vol. 24, pp. 337-357.
- 10) O.C. Zienkiewicz, J.Z. Zhu, The superconvergent patch recovery and *a posteriori* error estimates. Part 2: Error estimates and adaptivity. *International Journal for Numerical Methods in Engineering*, 1992, Vol. 33, pp. 1365-1382.
- 11) G.B. Sinclair, J.R. Beisheim, B.P. Epps, S.L. Pollice, Towards improved submodeling of stress concentrations. *Proceedings of the Ninth ANSYS Conference*, 2000, Pittsburgh, Pennsylvania, on CD-ROM.
- 12) M. Ainsworth, J.T. Oden, *A Posteriori Error Estimation in Finite Element Analysis*. John Wiley & Sons, Inc., 2000, New York, NY.
- 13) G.B. Sinclair, D. Mullan, A simple yet accurate finite element procedure for computing stress intensity factors. *International Journal for Numerical Methods in Engineering*, 1982, Vol. 18, pp. 1587-1600.
- 14) N.G. Cormier, B.S. Smallwood, G.B. Sinclair, G. Meda, Aggressive submodelling of stress concentrations. *International Journal for Numerical Methods in Engineering*, 1999, Vol. 46, pp. 889-909.

- 15) ANSYS personnel, *ANSYS Users' Manual* (Revision 9.0). ANSYS Inc., 2002, Canonsburg, Pennsylvania.
- 16) A.R. Zak, Stresses in the vicinity of boundary discontinuities in bodies of revolution. *Journal of Applied Mechanics*, 1964, Vol. 31, pp. 150-152.
- 17) Y. Lu, G.B. Sinclair, Numerical detection of stress singularities at reentrant corners. Report ME-MA6-05, 2005, Department of Mechanical Engineering, Louisiana State University, Baton Rouge, Louisiana.
- 18) C.W. Rummel, G.B. Sinclair, Finite element analysis of sharp corners with and without stress singularities: plane strain states. Report ME-MA4-05, 2005, Department of Mechanical Engineering, Louisiana State University, Baton Rouge, Louisiana.
- 19) H.R. Gadre, G.B. Sinclair, Finite element analysis of sharp corners with and without stress singularities: antiplane shear states. Report ME-MA3-05, 2005, Department of Mechanical Engineering, Louisiana State University, Baton Rouge, Louisiana.
- 20) S. Sezer, An assessment of ANSYS contact elements. *Proceedings of the Twelfth ANSYS Conference*, 2006, Pittsburgh, Pennsylvania, on CD-ROM.
- 21) R.D. Henshell, K.G. Shaw, Crack tip finite elements are unnecessary. *International Journal for Numerical Methods in Engineering*, 1975, Vol. 9, pp. 495-507.
- 22) R.S. Barsoum, On the use of isoparametric finite elements in linear fracture mechanics. *International Journal for Numerical Methods in Engineering*, 1976, Vol. 10, pp. 25-37.
- 23) R. Wait, Finite element methods for elliptic problems with singularities. *Computer Methods in Applied Mechanics and Engineering*, 1978, Vol. 13, pp. 141-150.
- 24) G.B. Sinclair, FEA of singular elasticity problems. *Proceedings of the Eighth ANSYS Conference*, 1998, Pittsburgh, Pennsylvania, Vol. 1, pp. 225-236.
- 25) D.B. Bogy, Two edge-bonded elastic wedges of different materials and wedge angles under surface tractions. *Journal of Applied Mechanics*, 1971, Vol. 38, pp. 377-386.
- 26) D.B. Bogy, On the problem of edge-bonded quarter-planes loaded at the boundary. *International Journal of Solids and Structures*, 1970, Vol. 6, pp. 1287-1313.
- 27) M.L. Williams, Stress singularities resulting from various boundary conditions in angular corners of plates in extension. *Journal of Applied Mechanics*, 1952, Vol. 19, pp. 526-528.
- 28) G.B. Sinclair, A.J. Birnbaum, J. Jiang, On the removal of stress singularities from bonded bimaterial interfaces. *Proceedings of Twentieth Canadian Congress of Applied Mechanics*, 2005, Montreal, Canada, pp. 527-528.
- 29) G.B. Sinclair, Y. Lu, J.A. Smouse, Practical convergence-divergence checks for stress analysis with finite elements. *Proceedings of the Twentieth Canadian Congress of Applied Mechanics*, 2005, Montreal, Canada, pp. 484-485.
- 30) G. Kolosoff, On some properties of the plane problem of elasticity theory. *Zeitschrift für Mathematik und Physik*, 1914, Vol. 62, pp. 384-409.
- 31) G.B. Sinclair, B.P. Epps, On the logarithmic stress singularities induced by the use of displacement shape functions in boundary conditions in submodelling. *Communications in Numerical Methods in Engineering*, 2002, Vol. 18, pp. 121-130.
- 32) S.P. Timoshenko, J.N. Goodier, *Theory of Elasticity* (3<sup>rd</sup> edition). McGraw-Hill Book Co., 1970, New York, NY.
- 33) E.R. Lewis, G.B. Sinclair, Test problems for finite element analysis of packing rings. Report ME-MA5-05, 2005, Department of Mechanical Engineering, Louisiana State University, Baton Rouge, Louisiana.
- 34) K.L. Johnson, *Contact Mechanics*. Cambridge University Press, 1985, Cambridge, England.
- 35) M. Ciavarella, D.A. Hills, G. Monno, The influence of rounded edges on indentation by a flat punch. *Proceedings of the Institution of Mechanical Engineers*, 1998, Vol 212C, pp. 319-328.

## Appendix A: Singular trial problems

Here we furnish further FEA results for peak stresses in the singular trial problems. We start by giving these stresses when a power singularity is present, then give these stresses when a logarithmic singularity is present.

For the ‘bimaterial’ plate with a right-angled reentrant corner under tension (Figure 3,  $\phi = 90^\circ$ ), we treat two other moduli ratios:  $E_+/E_- = 1, 4$ . The first of these is actually a single-material plate: We include results for this case because they enable comparison of the free-mesh FEA used here with a subsequent structured-mesh FEA. Singularity exponents for these two ratios are as in Table 14 wherein  $\gamma'$  is the exponent for the second weaker singularity which is also active when  $E_+/E_- = 4$  (from Williams, Reference 27, and Bogy, Reference 25, with  $\nu = 1/4$ ). Details of the FEA are given in Reference 17. Resulting normalized stresses, defined as in (48), are set out in the second and third columns of Table 15. In this table, the mesh number  $m$  is as in (49), and the numbers in parentheses are the moduli ratios.

Also included in Table 15 are peak stress results for a further butt joint under tension (Figure 4) when  $E_+/E_- = 20$ . The singularity exponent for this configuration is  $\gamma = 0.325$  (from Bogy, Reference 26, with  $\nu = 9/20$ ). The FEA is as described in the main body of the paper. Resulting stresses, defined as in (53), are given in the last column of Table 15.

**Table 14: Singularity exponents for bimaterial corners under tension**

$E_+/E_-$	$\gamma$	$\gamma'$
1	0.456	-
4	0.427	0.140

**Table 15:  $\bar{\sigma}_{\max}$  for bimaterial corners and a butt joint**

$m$	$\bar{\sigma}_{\max}(1)$	$\bar{\sigma}_{\max}(4)$	$\bar{\sigma}_{\max}(20)$
1	10.28	9.78	1.044
2	11.88	11.27	-
3	13.10	12.36	-
4	14.00	13.15	1.330
16	19.11	17.67	1.692
64	-	-	2.138

For a homogeneous elastic plate with a right-angled reentrant corner (Figure 3 with  $E_+ = E$  and  $\phi = 90^\circ$ ), the singularity exponent is as in Table 14 for tension ( $\sigma_0$ ), while  $\gamma = 1/3$  for antiplane shear ( $\tau_a$ ; Reference 4, Section 4.1) and  $\gamma$  is as in (55) for in-plane shear ( $\tau_0$ ). For other corners ( $\phi = 45^\circ, 135^\circ$ ), respective singularity exponents for  $\sigma_0, \tau_a$  and  $\tau_0$  are set out in Table 16 (from Williams, Reference 27, and Reference 4, Section 4.1). Details of the FEA for all three corners are given in References 18, 19. Resulting normalized stresses, defined as in (48) and (56), are set out for in-plane tension in the second, fourth, and fifth columns of Table 17a, while those for in-plane shear are set out in the third column.

Resulting normalized shear stresses, defined analogously to (56), are set out in Table 17b for antiplane shear. Throughout Table 17,  $m$  is as in (52) and numbers in parentheses are  $\phi$ .

**Table 16: Singularity exponents for reentrant corners**

$\phi$	$\gamma(\sigma_0)$	$\gamma(\tau_a)$	$\gamma(\tau_0)$
45°	0.495	0.429	0.340
135°	0.326	0.200	-

**Table 17a:  $\bar{\sigma}_{\max}, \bar{\tau}_{\max}$  for reentrant corners under in-plane tension, shear**

$m$	$\bar{\sigma}_{\max}(45^\circ)$	$\bar{\tau}_{\max}(45^\circ)$	$\bar{\sigma}_{\max}(90^\circ)$	$\bar{\sigma}_{\max}(135^\circ)$
1	73.00	10.48	17.77	5.258
2	110.8	13.73	25.39	6.690
3	161.4	17.63	35.46	8.422
4	231.3	22.41	49.02	10.56

**Table 17b:  $\bar{\tau}_{\max}^a$  for reentrant corners in antiplane shear**

$m$	$\bar{\tau}_{\max}^a(45^\circ)$	$\bar{\tau}_{\max}^a(90^\circ)$	$\bar{\tau}_{\max}^a(135^\circ)$
1	2.250	1.730	1.364
2	3.244	2.212	1.570
3	4.516	2.804	1.805

For flat-ended, rigid, smooth punches indenting an elastic half-space (Figure 9,  $r_e = 0$ ), inverse-square-root stress singularities occur at the edges of contact for both the strip punch (plane strain case; see, e.g., Reference 34, Section 2.8) and the right-circular cylindrical punch (axisymmetric case; see, e.g., Reference 34, Section 3.4). Details of the FEA for both flat-ended punches are given in Reference 20. Resulting normal contact stresses at the edges of contact, normalized by the average pressure and multiplied by  $-1$ , are set out in Tables 18a and 18b for the plane strain and axisymmetric cases, respectively. In Table 18,  $m$  is as in (52) and the parentheses contain designations of the host element used.

**Table 18a:  $\bar{\sigma}_{\max}$  for rigid, flat-ended, strip punch**

$m$	$\bar{\sigma}_{\max}$ (4Q)	$\bar{\sigma}_{\max}$ (8Q)
1	2.132	1.736
2	3.016	2.437
3	4.266	3.434

**Table 18b:  $\bar{\sigma}_{\max}$  for rigid, flat-ended, cylindrical punch**

$m$	$\bar{\sigma}_{\max}$ (4Q)	$\bar{\sigma}_{\max}$ (8Q)
1	1.641	1.321
2	2.347	1.884
3	3.338	2.678

Turning to trial problems with log singularities, Table 19 gives some results for log singularities induced by discontinuities in displacement derivatives in boundary conditions. In this table,  $m$  is as in (52) and parentheses contain nodal location designations. Details of these locations and the FEA producing these results may be found in Reference 31.

**Table 19a: Boundary stresses with displacement shape function conditions ( $K_T = 5.6$ )**

$m$	$\bar{\sigma}_x$ (N1)	$\bar{\sigma}_x$ (N2)	$\bar{\sigma}_y$ (N1)	$\bar{\sigma}_y$ (N2)
1	1.245	1.0550	5.483	5.678
2	1.198	1.0528	5.482	5.530
3	1.142	1.0495	5.472	5.398
4	1.081	1.0481	5.457	5.271

**Table 19b: Boundary stresses with displacement shape function conditions ( $K_T = 37.8$ )**

$m$	$\bar{\sigma}_x(N1')$	$\bar{\sigma}_x(N2')$	$\bar{\sigma}_y(N1')$	$\bar{\sigma}_y(N2')$
1	20.57	3.683	38.17	28.66
2	18.29	3.284	37.57	26.74
3	16.19	2.767	36.81	24.98

## Appendix B: Nonsingular test problems

Here we furnish further FEA results for selected key stresses in nonsingular test problems. We start by giving further stresses for polynomial problems, then give hoop stresses for thick-wall pressure vessels, then give additional peak stresses for elastic plates with elliptical holes, and thereafter close by giving further Hertzian and Steuermann contact stresses. Throughout the tables presenting these results, the mesh number  $m$  is as in (52) unless otherwise stated: thus mesh refinement as in (3) with  $\lambda = 2$ .

For the first-order and second-order polynomial problems stemming from (64) on the elastic plate of Figure 2, FEA stresses for 4Q elements are given in Table 20a. For second-order and third-order problems, stresses for 8Q elements are given in Table 20b (as expected, 8Q elements solve the first-order problem exactly and so results are omitted). For both element types,  $N_1 = 8$ . In these tables, the normalized stresses are defined by:

$$\begin{aligned}\bar{\sigma}_{x1} &= \sigma_{x1}(\text{at } x = 2l, y = 0) / \sigma_1 = 2 \\ \bar{\tau}_{xy1} &= -\tau_{xy1}(\text{at } x = 0, y = l) / \sigma_1 = 1 \\ \bar{\sigma}_{x2} &= -\sigma_{x2}(\text{at } x = 0, y = l) / \sigma_2 = 2 \\ \bar{\sigma}'_{x2} &= \sigma_{x2}(\text{at } x = 2l, y = 0) / \sigma_2 = 4 \\ \bar{\sigma}_{y2} &= \sigma_{y2}(\text{at } x = 0, y = 1) / \sigma_2 = 1\end{aligned}$$

and  $\bar{\sigma}_{x3}, \bar{\tau}_{xy3}$  are  $\bar{\sigma}_x, \bar{\tau}_{xy}$  of (65); here coordinates are as in Figure 2, and exact values follow from (64). In these definitions, the added numerical subscripts distinguish the order of problem.

**Table 20a: Stress results for first-order and second-order polynomial problems (4Q)**

$m$	$\bar{\sigma}_{x1}$	$\bar{\tau}_{xy1}$	$\bar{\sigma}_{x2}$	$\bar{\sigma}'_{x2}$	$\bar{\sigma}_{y2}$
1	1.7471	0.7486	2.0006	3.1273	0.6480
2	1.8746	0.8747	2.0319	3.5350	0.7866
3	1.9374	0.9375	2.0236	3.7590	0.8841
4	1.9688	0.9687	2.0137	3.8773	0.9398
5	1.9843	0.9844	2.0074	3.9381	0.9693

**Table 20b: Stress results for second-order and third-order polynomial problems (8Q)**

$m$	$\bar{\sigma}_{x2}$	$\bar{\sigma}'_{x2}$	$\bar{\sigma}_{y2}$	$\bar{\sigma}'_{x3}$	$\bar{\tau}_{xy3}$
1	2.0417	3.9583	0.9583	2.5133	7.7457
2	2.0105	3.9895	0.9896	1.3999	7.9390
3	2.0025	3.9975	0.9974	1.1006	7.9847
4	2.0007	3.9993	0.9994	1.0251	7.9962
5	2.0002	3.9998	0.9998	1.0063	7.9991

For the thick-wall pressure vessel problems (Figure 7), exact solutions for normalized hoop stresses,  $\bar{\sigma}_\theta$ , induced by an internal pressure  $p$  and at the outer radius  $r_o$  and inner radius  $r_i$ , are (see, e.g. Reference 32, Section 28):

$$\bar{\sigma}_\theta(r_o) = \sigma_\theta(\text{at } r = r_o)/p = 2\sqrt{\left[(r_o/r_i)^2 - 1\right]}$$

$$\bar{\sigma}_\theta(r_i) = \sigma_\theta(\text{at } r = r_i)/p = \bar{\sigma}_\theta(r_o) + 1$$

Two pressure vessels are analyzed with FEA in Reference 33: a thick-wall vessel with

$$(r_o/r_i)_1 = 53/39, \sigma_{\theta 1}(r_o) = 2.3618, \sigma_{\theta 1}(r_i) = 3.3618$$

and a vessel with a relatively thin wall with

$$(r_o/r_i)_2 = 27/26, \sigma_{\theta 2}(r_o) = 25.509, \sigma_{\theta 2}(r_i) = 26.509$$

Now numerical subscripts distinguish the radii ratio. Corresponding FEA results are set out in Table 21.

**Table 21: Hoop stresses for thick-wall pressure vessels**

$m$	$\bar{\sigma}_{\theta 1}(r_o)$	$\bar{\sigma}_{\theta 1}(r_i)$	$\bar{\sigma}_{\theta 2}(r_o)$	$\bar{\sigma}_{\theta 2}(r_i)$
1	2.3600	3.3662	25.372	26.628
2	2.3611	3.3641	25.476	26.540
3	2.3619	3.3634	25.496	26.522

For plates with elliptical holes with varying aspect ratios under tension (Figure 8), Table 22 gives  $\bar{\sigma}_{\max} = K_T, \sigma_{\max}$  as in (72), from FEA with structured 4Q and 8Q meshes, and a free mesh of four-node quadrilaterals distinguished as 4Q' in Tables 22a, b. Also in Table 22b,  $\bar{\sigma}'_{\max}$  distinguishes  $\bar{\sigma}_{\max}$  for  $K_T = 105.31$ . Details of the FEA producing these results may be found in Reference 11.

**Table 22a:  $\bar{\sigma}_{\max}$  for plate with elliptical hole under tension ( $K_T = 5.61$ )**

$m$	$\bar{\sigma}_{\max} (4Q)$	$\bar{\sigma}_{\max} (4Q')$	$\bar{\sigma}_{\max} (8Q)$
1	5.5550	5.4459	5.6329
2	5.5955	5.5640	5.6159
3	5.6063	5.5978	5.6113

**Table 22b:  $\bar{\sigma}_{\max}$  for plate with elliptical holes under tension ( $K_T = 37.88, 105.31$ )**

$m$	$\bar{\sigma}_{\max} (4Q)$	$\bar{\sigma}_{\max} (4Q')$	$\bar{\sigma}_{\max} (8Q)$	$\bar{\sigma}'_{\max} (8Q)$
1	27.533	6.5387	29.607	47.991
2	33.534	9.9665	35.476	70.802
3	36.447	15.835	37.472	91.480
4	37.469	23.652	37.788	102.18
5	37.770	30.680	37.847	104.70

**Table 22c:  $\bar{\sigma}_{\max}$  for plate with elliptical hole under tension ( $K_T = 296.04$ )**

$m$	$\bar{\sigma}_{\max} (4Q)$	$\bar{\sigma}_{\max} (8Q)$
1	53.826	60.303
2	94.715	105.86
3	152.27	166.11
4	215.02	230.04
5	261.84	275.92
6	284.71	292.11
7	292.78	295.05
8	295.17	-

For plates with elliptical holes with varying aspect ratios under tension, Table 23 gives  $\bar{\sigma}_{\max}$  from FEA with free meshes of four-node quadrilaterals that are adaptively refined, denoted by 4Qa therein. The number of elements in initial coarse grids,  $N_1$ , given in parentheses, is set by the scale factor implicit in  $N_2, N_3$  for two refined grids. Hence

$$N_1 = N_2^2 / N_3$$

This leads to effective scale factors of  $\lambda = 1.72, 1.67$  in Table 23a,  $\lambda = 1.77, 2.14$  in Table 23b, and  $\lambda = 2.07, 1.77$  in Table 23c. Thus scale factors all in excess of 1.5, the minimum value. Corresponding  $\bar{\sigma}_{\max}$  for  $N_1$ , given in parentheses, are estimated simply by linear interpolation. The results needed for this interpolation, as well as details of the FEA producing them, may be found in Reference 11.

**Table 23a:  $\bar{\sigma}_{\max}$  for plate with elliptical hole under tension ( $K_T = 37.88, 4Qa$ )**

$N$	$\bar{\sigma}_{\max}$	$N$	$\bar{\sigma}_{\max}$
(660)	(4.5)	(2,096)	(31.6)
1,961	31.4	5,830	37.3
5,830	37.3	16,214	37.8

**Table 23b:  $\bar{\sigma}_{\max}$  for plate with elliptical hole under tension ( $K_T = 105.31, 4Qa$ )**

$N$	$\bar{\sigma}_{\max}$	$N$	$\bar{\sigma}_{\max}$
(1,403)	(10.9)	(3,047)	(46.4)
4,420	68.6	13,920	98.9
13,920	98.9	63,585	104.9

**Table 23c:  $\bar{\sigma}_{\max}$  for plate with elliptical hole under tension ( $K_T = 296.04, 4Qa$ )**

$N$	$\bar{\sigma}_{\max}$	$N$	$\bar{\sigma}_{\max}$
(11,967)	(128.9)	(70,073)	(250.9)
51,128	245.8	218,448	290.6
218,448	290.6	681,000	295.2

For Hertzian cylindrical contact (Figure 9,  $w = 0$ ), Table 24 gives peak normalized stresses from FEA with uniform 4Q and 8Q meshes and  $N_1 = 256$ . Details of the FEA producing these results may be found in Reference 20. In Table 24, the normalized stresses are defined by:

$$\bar{\sigma}_c = -\sigma_z (\text{at } x = 0, z = 0) / p = 4/\pi$$

$$\bar{\sigma}_h = -\sigma_x (\text{at } x = 0, z = 0) / p = 4/\pi$$

where coordinates are as in Figure 9 and exact values are from Reference 34, Section 4.2(c).

**Table 24: Contact stresses for Hertzian cylindrical contact**

$m$	$\bar{\sigma}_c$ (4Q)	$\bar{\sigma}_c$ (8Q)	$\bar{\sigma}_h$ (4Q)	$\bar{\sigma}_h$ (8Q)
1	1.2628	1.2961	1.2119	1.2188
2	1.2704	1.2809	1.2214	1.2216
3	1.2737	1.2761	1.2241	1.2237

For Steuermann contact (Figure 9), Table 25 gives peak, normalized, contact stresses,  $\bar{\sigma}_c$  of (74), for three different degrees of edge roundness ( $w/r_e$  in parentheses), with two load levels for the least round ( $w/r_e = 7$ ). Poisson's ratio for results in the second through fourth columns is  $\frac{1}{4}$ ; Poisson's ratio for the fifth column is 0.42. These are from FEA with nonuniform 4Q meshes. Initial element numbers are  $N_1 = 8000$ , 16,000, 17,000 and 2000 for the second, third, fourth and fifth column results of Table 25, respectively. Details of the FEA producing the results in second through fourth column may be found in Reference 20. Corresponding exact solutions from Steuermann (as reported in Reference 35) are:

$$w/r_e = 1, p/E = 1/1000, \bar{\sigma}_c = 9.9773$$

$$w/r_e = 3, p/E = 1/1000, \bar{\sigma}_c = 10.957$$

$$w/r_e = 7, p/E = 1/1000, \bar{\sigma}_c = 13.175$$

$$w/r_e = 7, p/E = 1/2455, \bar{\sigma}'_c = 17.372$$

**Table 25: Contact stresses for Steuermann contact**

$m$	$\bar{\sigma}_c$ (1)	$\bar{\sigma}_c$ (3)	$\bar{\sigma}_c$ (7)	$\bar{\sigma}'_c$ (7)
1	9.3506	9.9830	11.834	13.454
2	9.7120	10.618	12.560	16.195
3	9.8500	10.832	12.707	16.947